Supplementary Information:

Plasma-Catalytic Ammonia Synthesis in a DBD Plasma: Role of the Micro-Discharges and Their Afterglows

K. van ‘t Veer[1,2,*], Y. Engelmann[1], F. Reniers[2], A. Bogaerts[1,*]

[1]*University of Antwerp, Department of Chemistry, Research Group PLASMANT, Universiteitsplein 1, 2610 Wilrijk-Antwerp, Belgium*

[2] *Université Libre de Bruxelles, Faculty of Sciences, Chemistry of Surfaces, Interfaces and Nanomaterials, CP255, Avenue F. D. Roosevelt 50, B-1050 Brussels, Belgium*

[*]E-mail: kevin.vantveer@uantwerpen.be, annemie.bogaerts@uantwerpen.be

S.1. Description of the Model

We used a time-dependent 0D plasma kinetics model[1,2] to investigate a PB DBD. The principles to capture the properties of a PB DBD in a 0D model are already described in our previous work.[3] We list the chemical reactions in the plasma and at the surface in section S.1.1. In contrast to our previous work, we now derive the plasma conditions more directly from experimentally measured current and voltage characteristics of a PB DBD, as described in section S.1.2 and S.1.3.

S.1.1. Plasma Kinetic and Surface Kinetic Reactions

Table S1 through S5 report all the gas phase reactions included in the model. In table S1, the electron-impact reactions are reported, most of which are evaluated from a unique cross section (i.e. $\sigma(\epsilon)$, with ϵ the electron energy) and the electron energy distribution function, which is calculated in the model with BOLSIG+.[2] Each cross section has a different threshold energy, which describes the onset of the reaction. For example, the threshold energy of N_2 dissociation is higher than of H_2 dissociation (9.8 eV and 4.5 eV, respectively).[4] Table S5 reports the included vibrational interactions of the feed gas molecules. Table S6 reports the surface kinetics, followed by a small discussion on the parameters describing those reactions.

Table S1. Electron-impact collisions describing the plasma kinetics. The ground state, vibrational levels and electronically excited states are indicated with X, V and E, respectively. The temperatures are given in Kelvin unless otherwise noted.

#	Reaction	Rate coefficient	Ref.	
	Excitation and de-excitation			
R1	$e^- + H_2(X,V) \leftrightarrow e^- + H_2(E)$	$\sigma_{R1}(\epsilon)$	[5]	[1,2,3]
R2	$e^- + N_2(X,V) \leftrightarrow e^- + N_2(E)$	$\sigma_{R2}(\epsilon)$	[5]	[1,2,3]
R3	$e^- + N \rightarrow e^- + N(E)$	$\sigma_{R3}(\epsilon)$	[5]	[1]
	Ionization			
R4	$e^- + N_2(X,V,E) \rightarrow e^- + e^- + N_2^+$	$\sigma_{R4}(\epsilon)$	[6]	[1,2]
R5	$e^- + H_2(X,V) \rightarrow e^- + e^- + H_2^+$	$\sigma_{R5}(\epsilon)$	[5]	[1,2]
R6	$e^- + N \rightarrow e^- + e^- + N^+$	$\sigma_{R6}(\epsilon)$	[5]	[1]

R7	$e^- + H$	→	$e^- + e^- + H^+$	$\sigma_{R7}(\epsilon)$	6	1
R8	$e^- + NH$	→	$e^- + e^- + NH^+$	$\sigma_{R8}(\epsilon)$	7	1
R9	$e^- + NH_2$	→	$e^- + e^- + NH_2^+$	$\sigma_{R9}(\epsilon)$	7	1
R10	$e^- + NH_3$	→	$e^- + e^- + NH_3^+$	$\sigma_{R10}(\epsilon)$	7	1
	Dissociative Ionization					
R11	$e^- + N_2(X,V)$	→	$e^- + e^- + N^+ + N$	$\sigma_{R11}(\epsilon)$	8	1
R12	$e^- + H_2$	→	$e^- + e^- + H + H^+$	$\sigma_{R12}(\epsilon)$	9	1
R13	$e^- + NH$	→	$e^- + e^- + H + N^+$	$\sigma_{R13}(\epsilon)$	7	1
R14	$e^- + NH_2$	→	$e^- + e^- + H + NH^+$	$\sigma_{R14}(\epsilon)$	7	1
R15	$e^- + NH_3$	→	$e^- + e^- + H + NH_2^+$	$\sigma_{R15}(\epsilon)$	7	1
	Dissociation					
R16	$e^- + H_2$	→	$e^- + H + H$	$\sigma_{R16}(\epsilon)$	9	1
R17	$e^- + N_2(X,V,E)$	→	$e^- + N + N$	$\sigma_{R17}(\epsilon)$	5	1,2
R18	$e^- + NH$	→	$e^- + N + H$	$5.0 \times 10^{-8}\, T_e[\mathrm{eV}]^{0.5} \exp(-8.6/T_e[\mathrm{eV}])$	10	
R19	$e^- + NH_2$	→	$e^- + N + H_2$	$5.0 \times 10^{-8}\, T_e[\mathrm{eV}]^{0.5} \exp(-7.6/T_e[\mathrm{eV}])$	10	
R20	$e^- + NH_2$	→	$e^- + NH + H$	$5.0 \times 10^{-8}\, T_e[\mathrm{eV}]^{0.5} \exp(-7.6/T_e[\mathrm{eV}])$	10	
R21	$e^- + NH_3$	→	$e^- + NH_2 + H$	$5.0 \times 10^{-8}\, T_e[\mathrm{eV}]^{0.5} \exp(-4.4/T_e[\mathrm{eV}])$	10	
R22	$e^- + NH_3$	→	$e^- + NH + H_2$	$5.0 \times 10^{-8}\, T_e[\mathrm{eV}]^{0.5} \exp(-5.5/T_e[\mathrm{eV}])$	10	
	(Dissociative) recombination					
R23	$e^- + N_2^+$	→	$N + N$	$0.50 \times 1.8 \times 10^{-7}(300/T_e)^{0.39}$	11	
R24	$e^- + N_2^+$	→	$N + N(^2D^0)$	$0.45 \times 1.8 \times 10^{-7}(300/T_e)^{0.39}$	11	
R25	$e^- + N_2^+$	→	$N + N(^2P^0)$	$0.05 \times 1.8 \times 10^{-7}(300/T_e)^{0.39}$	11	
R26	$e^- + N_3^+$	→	$N_2 + N$	$2.0 \times 10^{-7}(300/T_e)^{0.5}$	11	
R27	$e^- + N_3^+$	→	$N_2(A^3) + N$	$6.91 \times 10^{-8} T_e[\mathrm{eV}]^{-0.5}$	12	
R28	$e^- + N_3^+$	→	$N_2(B^3) + N$	$6.91 \times 10^{-8} T_e[\mathrm{eV}]^{-0.5}$	12	
R29	$e^- + N_4^+$	→	$N_2 + N_2$	$2.3 \times 10^{-6}(300/T_e)^{0.53}$	11	
R30	$e^- + N_4^+$	→	$N_2 + N + N$	$3.13 \times 10^{-7} T_e[\mathrm{eV}]^{-0.41}$	12	
R31	$e^- + H_2^+$	→	$H + H$	see footnote[4]	10	4
R32	$e^- + H_3^+$	→	$H + H + H$	see footnote[5]	10	5
R33	$e^- + H_3^+$	→	$H_2 + H$	see footnote[5]	10	5
R34	$e^- + NH^+$	→	$N + H$	$4.30 \times 10^{-8}(0.026/T_e[\mathrm{eV}])^{0.5}$	10	
R35	$e^- + NH_2^+$	→	$NH + H$	$1.02 \times 10^{-7}(0.026/T_e[\mathrm{eV}])^{0.4}$	10	
R36	$e^- + NH_2^+$	→	$N + H + H$	$1.98 \times 10^{-7}(0.026/T_e[\mathrm{eV}])^{0.4}$	10	
R37	$e^- + NH_3^+$	→	$NH + H + H$	$1.55 \times 10^{-7}(0.026/T_e[\mathrm{eV}])^{0.5}$	10	
R38	$e^- + NH_3^+$	→	$NH_2 + H$	$1.55 \times 10^{-7}(0.026/T_e[\mathrm{eV}])^{0.5}$	10	
R39	$e^- + NH_4^+$	→	$NH_3 + H$	$8.01 \times 10^{-7}(0.026/T_e[\mathrm{eV}])^{0.605}$	10	
R40	$e^- + NH_4^+$	→	$NH_2 + H + H$	$1.23 \times 10^{-7}(0.026/T_e[\mathrm{eV}])^{0.605}$	10	
R41	$e^- + N_2H^+$	→	$N_2 + H$	$7.1 \times 10^{-7}(0.026/T_e[\mathrm{eV}])^{0.72}$	10	
	Three-body recombination					

R42	$e^- + N^+ + e^- \rightarrow N + e^-$	$7.0 \times 10^{-20}(300/T_e)^{4.5}$	11	
R43	$e^- + N^+ + M \rightarrow N + M$	$6.0 \times 10^{-27}(300/T_e)^{1.5}$	13	6
R44	$e^- + N_2^+ + e^- \rightarrow N_2 + e^-$	$1.0 \times 10^{-19}(T_e/300)^{-4.5}$	13	
R45	$e^- + N_2^+ + M \rightarrow N_2 + M$	$2.49 \times 10^{-29} T_e[\mathrm{eV}]^{-1.5}$	12	6
	Attachment			
R46	$e^- + H_2(X,V) \rightarrow H + H^-$	$\sigma_{R46}(\epsilon)$	14,15	1,7

[1] The rate coefficient is calculated from the electron impact cross section $\sigma(\epsilon)$ using BOLSIG+.[2] The reference of the cross section is given.

[2] The cross section threshold energy is reduced when the reaction takes places from an excited state.

[3] The rate coefficients for de-excitation processes are calculated using detailed balancing.[2]

[4] The rate coefficient is a fit as a function of the electron temperature, given by: $k = 7.51 \times 10^{-9} - 1.12 \times 10^{-9} T_e[\mathrm{eV}]^1 + 1.03 \times 10^{-10} T_e[\mathrm{eV}]^2 - 4.15 \times 10^{-12} T_e[\mathrm{eV}]^3 + 5.86 \times 10^{-14} T_e[\mathrm{eV}]^4$.[10]

[5] The rate coefficient is a fit as a function of the electron temperature, given by: $k = 0.5 \times (8.39 \times 10^{-9} + 3.02 \times 10^{-9} T_e[\mathrm{eV}]^1 - 3.80 \times 10^{-10} T_e[\mathrm{eV}]^2 + 1.31 \times 10^{-11} T_e[\mathrm{eV}]^3 + 2.42 \times 10^{-13} T_e[\mathrm{eV}]^4 - 2.30 \times 10^{-14} T_e[\mathrm{eV}]^5 + 3.55 \times 10^{-16} T_e[\mathrm{eV}]^6)$.[10]

[6] The third body, M, is any neutrally charged gas phase species.

[7] The cross section data is resolved for each individual vibrational state.[14,15]

Table S2 Neutral-neutral collisions describing the plasma kinetics. The ground state and vibrational levels are indicated with X and V, respectively. The temperatures are given in Kelvin.

#	**Reaction**	**Rate coefficient**	**Ref.**	
	Neutral-neutral collisions			
R47	$N_2(X,V) + M \rightarrow N + N + M$	$8.37 \times 10^{-4}(T_g/298)^{-3.50} \exp(-113710/T_g)$	16	1,2
R48	$N(^2D^0) + M \rightarrow N + M$	2.4×10^{-14}	17	2
R49	$N(^2P^0) + N \rightarrow N(^2D^0) + N$	1.8×10^{-12}	11	
R50	$N(^2P^0) + N_2 \rightarrow N + N_2$	2.0×10^{-18}	11	
R51	$N_2(a'^1) + N \rightarrow N_2 + N$	2.0×10^{-11}	17	
R52	$N_2(a'^1) + N_2 \rightarrow N_2 + N_2$	3.7×10^{-16}	17	
R53	$N_2(a'^1) + N_2 \rightarrow N_2(B^3) + N_2$	1.9×10^{-13}	11	
R54	$N_2(A^3) + N \rightarrow N_2 + N(^2P^0)$	$4.0 \times 10^{-11}(300/T_g)^{0.667}$	11	
R55	$N_2(A^3) + N \rightarrow N_2 + N$	2.0×10^{-12}	11	
R56	$N_2(A^3) + N_2 \rightarrow N_2 + N_2$	3.0×10^{-16}	11	
R57	$N_2(A^3) + N_2(A^3) \rightarrow N_2 + N_2(A^3)$	2.0×10^{-12}	17	
R58	$N_2(A^3) + N_2(A^3) \rightarrow N_2 + N_2(B^3)$	3.0×10^{-10}	11	
R59	$N_2(A^3) + N_2(A^3) \rightarrow N_2 + N_2(C^3)$	1.5×10^{-10}	11	
R60	$N_2(B^3) + N_2 \rightarrow N_2 + N_2$	2.0×10^{-12}	11	
R61	$N_2(B^3) + N_2 \rightarrow N_2(A^3) + N_2$	3.0×10^{-11}	11	
R62	$N_2(C^3) + N_2 \rightarrow N_2(a'^1) + N_2$	1.0×10^{-11}	11	
R63	$N + NH \rightarrow H + N_2$	5×10^{-11}	18	
R64	$H + NH \rightarrow N + H_2$	$5.4 \times 10^{-11} \exp(-165/T_g)$	18	

R65	$NH + NH$	→	$H_2 + N_2$	$5 \times 10^{-14}(T_g/300)$	18	3
R66	$NH + NH$	→	$N + NH_2$	$1.7 \times 10^{-12}(T_g/300)^{1.5}$	18	3
R67	$NH + NH$	→	$N_2 + H + H$	8.5×10^{-11}	18	3
R68	$H + NH_2$	→	$H_2 + NH$	$6.6 \times 10^{-11} \exp(-1840/T_g)$	18	
R69	$N + NH_2$	→	$N_2 + H + H$	1.2×10^{-10}	18	
R70	$N + NH_2$	→	$N_2 + H_2$	1.2×10^{-10}	18	
R71	$NH + NH_2$	→	$NH_3 + N$	1.66×10^{-12}	18	4
R72	$H_2(V) + N$	→	$NH + H$	$4.0 \times 10^{-10}(T_g/300)^{0.5} \exp(-16600/T_g)$	18	5
R73	$H_2 + NH_2$	→	$NH_3 + H$	$5.4 \times 10^{-11} \exp(-6492/T_g)$	18	
R74	$H + NH_3$	→	$NH_2 + H_2$	$8.4 \times 10^{-14}(T_g/300)^{4.1} \exp(-4760/T_g)$	18	
R75	$N_2(A^3) + H$	→	$N_2 + H$	5×10^{-11}	18	
R76	$N_2(A^3) + H_2$	→	$N_2 + H + H$	$2 \times 10^{-10} \exp(-3500/T_g)$	18	
R77	$N_2(A^3) + NH_3$	→	$N_2 + NH_3$	1.6×10^{-10}	18	
R78	$N_2(B^3) + H_2$	→	$N_2(A^3) + H_2$	2.5×10^{-11}	18	
R79	$N_2(a'^1) + H$	→	$N_2 + H$	1.5×10^{-11}	18	
R80	$N_2(a'^1) + H_2$	→	$N_2 + H + H$	2.6×10^{-11}	18	
R81	$N + H_2(E)$	→	$H + NH$	$4.0 \times 10^{-10}(T_g/300)^{0.5}$	18	
R82	$N(^2D^0) + H_2$	→	$H + NH$	2.3×10^{-12}	18	
R83	$N(^2D^0) + NH_3$	→	$NH + NH_2$	1.1×10^{-10}	18	
R84	$N(^2P^0) + H_2$	→	$H + NH$	2.5×10^{-14}	18	
R85	$N + NH$	→	$H + N + N$	$4.02 \times 10^{-10}(T_g/298)^{-0.20} \exp(-27303/T_g)$	19	
R86	$H_2 + NH$	→	$H + NH_2$	$3.50 \times 10^{-11} \exp(-7758/T_g)$	20	
R87	$N_2 + H$	→	$NH + N$	$5.27 \times 10^{-10}(T_g/298)^{-0.50} \exp(-74453/T_g)$	19	
R88	$NH_2 + N$	→	$NH + NH$	$2.99 \times 10^{-13} \exp(-7600/T_g)$	21	
R89	$NH_2 + NH_2$	→	$NH_3 + NH$	$5.07 \times 10^{-15}(T_g/298)^{-3.53} \exp(-278/T_g)$	22	
R90	$NH_3 + NH$	→	$NH_2 + NH_2$	$2.33 \times 10^{-14}(T_g/298)^{-3.41} \exp(-7350/T_g)$	22	
R91	$H_2 + H$	→	$H + H + H$	$2.54 \times 10^{-8}(T_g/298)^{-0.10} \exp(-52561/T_g)$	23	
R92	$H_2 + N_2$	→	$H + H + N_2$	$2.61 \times 10^{-8}(T_g/298)^{-1.40} \exp(-52561/T_g)$	23	
R93	$H_2 + H_2$	→	$H + H + H_2$	$2.61 \times 10^{-8}(T_g/298)^{-0.70} \exp(-52561/T_g)$	23	
R94	$NH + M$	→	$H + N + M$	$2.99 \times 10^{-10} \exp(-37647/T_g)$	24	
R95	$NH_2 + M$	→	$H + NH + M$	$1.99 \times 10^{-9} \exp(-38248/T_g)$	24	
R96	$NH_3 + M$	→	$H + NH_2 + M$	$4.17 \times 10^{-8} \exp(-47149/T_g)$	25	6
R97	$NH_3 + M$	→	$H_2 + NH + M$	$1.05 \times 10^{-9} \exp(-47029/T_g)$	25	6
	Three-body collisions					
R98	$N + N + M$	→	$N_2 + M$	$1.38 \times 10^{-33} \exp(502.978/T_g)$	26	2

R99	$N + N + N$	→	$N_2(A^3) + N$	1.0×10^{-32}	[11]	
R100	$N + N + N$	→	$N_2(B^3) + N$	1.4×10^{-32}	[11]	
R101	$N + N + N_2$	→	$N_2(A^3) + N_2$	1.7×10^{-33}	[11]	
R102	$N + N + N_2$	→	$N_2(B^3) + N_2$	2.4×10^{-33}	[11]	
R103	$N + N + H_2$	→	$N_2 + H_2$	$(1/380) \times 8.3 \times 10^{-34} \exp(500/T_g)$	[18]	[7]
R104	$H + H + N_2$	→	$H_2 + N_2$	$(1/380) \times 8.3 \times 10^{-33}(300/T_g)$	[18]	[7]
R105	$H + N + M$	→	$NH + M$	$(1/380) \times 1.0 \times 10^{-33}$	[18]	[7,8]
R106	$N + H_2 + M$	→	$NH_2 + M$	$(1/380) \times 1.0 \times 10^{-34}$	[18]	[7,8]
R107	$H + NH + M$	→	$NH_2 + M$	$(1/380) \times 1.0 \times 10^{-32}$	[18]	[7,8]
R108	$H + NH_2 + M$	→	$NH_3 + M$	$(1/380) \times 5.5 \times 10^{-30}$	[18]	[7,8]
R109	$NH + H_2 + M$	→	$NH_3 + M$	$(1/380) \times 2.5 \times 10^{-35}(T_g/300) \exp(1700/T_g)$	[18]	[7,8]
R110	$N + N + H_2$	→	$N_2(A^3) + H_2$	$(1/380) \times 1.7 \times 10^{-33}$	[18]	[7]
R111	$N + N + H$	→	$N_2(A^3) + H$	$(1/380) \times 1.0 \times 10^{-32}$	[18]	[7]
R112	$N + N + H_2$	→	$N_2(B^3) + H_2$	$(1/380) \times 2.4 \times 10^{-33}$	[18]	[7]
R113	$N + N + H$	→	$N_2(B^3) + H$	$(1/380) \times 1.4 \times 10^{-32}$	[18]	[7]
R114	$H + H + H_2$	→	$H_2 + H_2$	$(1/380) \times 8.8 \times 10^{-33}(300/T_g)^{0.6}$	[18]	[7]
	Ionization processes					
R115	$N + N$	→	$e^- + N_2^+$	$2.7 \times 10^{-11} \exp(-67400/T_g)$	[11]	
R116	$N_2(a'^1) + N_2(a'^1)$	→	$e^- + N_2^+ + N_2$	5.0×10^{-13}	[17]	
R117	$N_2(a'^1) + N_2(a'^1)$	→	$e^- + N_4^+$	1.0×10^{-11}	[11]	
R118	$N_2(a'^1) + N_2(a'^1)$	→	$e^- + N_4^+$	4.0×10^{-12}	[11]	
R119	$N_2(A^3) + N_2(a'^1)$	→	$e^- + N_2^+ + N_2$	1.0×10^{-12}	[17]	
	Radiative decay					
R120	$N_2(A^3)$	→	N_2	0.5	[11]	
R121	$N_2(B^3)$	→	$N_2(A^3)$	1.34×10^5	[11]	
R122	$N_2(a'^1)$	→	N_2	1.0×10^2	[11]	
R123	$N_2(C^3)$	→	$N_2(B^3)$	2.45×10^7	[11]	

---

[1] The rate coefficient is scaled according to the Fridmann-Macheret alpha-model[27] with $\alpha = 1$.[16]

[2] The third body, M, is any neutrally charged gas phase species.

[3] R65, R66 and R67, are adopted from reference 18, however the product channel R65 can be considered very unlikely, as also reflected by the rate coefficients.

[4] A more likely reaction channel is $NH + NH_2 \rightarrow N_2H_2 + H$, however the N_2H_2 species is not described in our model.

[5] The reaction only occurs for the vibrational levels.[18] The reported rate coefficient is scaled according to the Fridmann-Macheret alpha-model[27] with $\alpha = 0.3$.[18]

[6] The adopted rate coefficients of R96 and R97 are related by $k_{R96}/k_{R97} \approx 40$, following the recommendations of Hanson et al.[25]

[7] The rate coefficients of the three-body collisions are multiplied by (1⁄380) to account for the reaction taking place at atmospheric pressure,[28] opposed to low pressure.[18]

[8] The third body, M, is $N_2(X)$, $N_2(V)$, $H_2(X)$ or $H_2(V)$.

Table S3. Ion-neutral collisions describing the plasma kinetics. The ground state and vibrational levels are indicated with X and V, respectively. The effective ion temperature T_{ion} [11] is given in Kelvin.

#	Reaction			Rate coefficient	Ref.
	Ion-neutral collisions				
R124	$N^+ + H_2$	→	$NH^+ + H$	5.0×10^{-10}	29
R125	$N^+ + NH_3$	→	$NH_2^+ + NH$	$0.20 \times 2.35 \times 10^{-9}$	29
R126	$N^+ + NH_3$	→	$NH_3^+ + N$	$0.71 \times 2.35 \times 10^{-9}$	29
R127	$N^+ + NH_3$	→	$N_2H^+ + H_2$	$0.09 \times 2.35 \times 10^{-9}$	29
R128	$N_2^+ + N$	→	$N^+ + N_2$	$7.2 \times 10^{-13}(T_{ion}/300)$	11
R129	$N_2^+ + H_2$	→	$N_2H^+ + H$	2.00×10^{-9}	10
R130	$N_2^+ + N_2(A^3)$	→	$N_3^+ + N$	3.0×10^{-10}	30
R131	$N_2^+ + NH_3$	→	$NH_3^+ + N_2$	1.95×10^{-9}	10
R132	$N_3^+ + N$	→	$N_2^+ + N_2$	6.6×10^{-11}	11
R133	$N_4^+ + N$	→	$N^+ + N_2 + N_2$	1.0×10^{-11}	11
R134	$N_4^+ + N_2$	→	$N_2^+ + N_2 + N_2$	$2.1 \times 10^{-16} \exp(T_{ion}/121)$	11
R135	$H^+ + NH_3$	→	$NH_3^+ + H$	5.20×10^{-9}	29
R136	$H_2^+ + H$	→	$H^+ + H_2$	6.4×10^{-10}	10
R137	$H_2^+ + H_2$	→	$H_3^+ + H$	2.0×10^{-9}	10
R138	$H_2^+ + N_2$	→	$N_2H^+ + H$	2.00×10^{-9}	29
R139	$H_2^+ + NH_3$	→	$NH_3^+ + H_2$	5.70×10^{-9}	29
R140	$NH^+ + H_2$	→	$H_3^+ + N$	$0.15 \times 1.23 \times 10^{-9}$	29
R141	$NH^+ + H_2$	→	$NH_2^+ + H$	$0.85 \times 1.23 \times 10^{-9}$	29
R142	$NH^+ + NH_3$	→	$NH_3^+ + NH$	$0.75 \times 2.40 \times 10^{-9}$	29
R143	$NH^+ + NH_3$	→	$NH_4^+ + N$	$0.25 \times 2.40 \times 10^{-9}$	29
R144	$NH^+ + N_2$	→	$N_2H^+ + N$	6.50×10^{-10}	29
R145	$NH_2^+ + H_2$	→	$NH_3^+ + H$	1.95×10^{-10}	29
R146	$NH_2^+ + NH_3$	→	$NH_3^+ + NH_2$	$0.5 \times 2.30 \times 10^{-9}$	29
R147	$NH_2^+ + NH_3$	→	$NH_4^+ + NH$	$0.5 \times 2.30 \times 10^{-9}$	29
R148	$NH_3^+ + NH_3$	→	$NH_4^+ + NH_2$	2.10×10^{-9}	29
R149	$N_2H^+ + NH_3$	→	$NH_4^+ + N_2$	2.3×10^{-9}	29
	Ion-neutral three-body collisions				
R150	$N_2^+ + N + N_2$	→	$N_3^+ + N_2$	$9.0 \times 10^{-30} \exp(400/T_{ion})$	11
R151	$N^+ + N_2 + N_2(X, V)$	→	$N_3^+ + N_2$	$1.7 \times 10^{-29}(300/T_{ion})^{2.1}$	11
R152	$N_2^+ + N_2 + N_2(X, V)$	→	$N_4^+ + N_2$	$5.2 \times 10^{-29}(300/T_{ion})^{2.2}$	11
R153	$N^+ + N + N_2$	→	$N_2^+ + N_2$	1.0×10^{-29}	11

Table S4. Negative-positive ion recombination reactions describing the plasma kinetics. The ground state and vibrational levels are indicated with X and V, respectively. The temperatures are given in Kelvin.

#	Reaction	Rate coefficient	Ref.
	H^- recombination		
R154	$H^- + H_2^+ \rightarrow H + H + H$	$2.0 \times 10^{-7}(300/T_g)$	18
R155	$H^- + H_3^+ \rightarrow H_2 + H + H$	$2.0 \times 10^{-7}(300/T_g)$	18
R156	$H^- + N_2^+ \rightarrow N_2 + H$	$2.0 \times 10^{-7}(300/T_g)$	18
R157	$H^- + N_4^+ \rightarrow N_2 + N_2 + H$	$2.0 \times 10^{-7}(300/T_g)$	18
R158	$H^- + N_2H^+ \rightarrow H_2 + N_2$	$2.0 \times 10^{-7}(300/T_g)$	18
	H^- three-body recombination		
R159	$H^- + H_2^+ + M \rightarrow H_2 + H + N_2$	$(1/380) \times 2 \times 10^{-25}(300/T_g)^{2.5}$	18 [1,2]
R160	$H^- + H_3^+ + M \rightarrow H_2 + H_2 + M$	$(1/380) \times 2 \times 10^{-25}(300/T_g)^{2.5}$	18 [1,2]
R161	$H^- + N_2^+ + M \rightarrow N_2 + H + M$	$(1/380) \times 2 \times 10^{-25}(300/T_g)^{2.5}$	18 [1,2]
R162	$H^- + N_4^+ + M \rightarrow N_2 + N_2 + H + M$	$(1/380) \times 2 \times 10^{-25}(300/T_g)^{2.5}$	18 [1,2]
R163	$H^- + N_2H^+ + M \rightarrow H_2 + N_2 + M$	$(1/380) \times 2 \times 10^{-25}(300/T_g)^{2.5}$	18 [1,2]

[1] The rate coefficients of the three-body collisions are multiplied by (1⁄380) to account for the reaction taking place at atmospheric pressure,[28] opposed to low pressure.[18]

[2] The third body, M, is $N_2(X)$, $N_2(V)$, $H_2(X)$ or $H_2(V)$.

Table S5. Vibrational processes describing the plasma kinetics. The calculations of the rate coefficients can be found in the listed references.

#	Reaction		Ref.
	Excitation and de-excitation		
R164	$e + N_2(v) \leftrightarrow N_2(v' > v) + e$	$v = 1 \ldots 24$	15
R165	$e + H_2(v) \leftrightarrow H_2(v' > v) + e$	$v = 1 \ldots 14$	31,32
	Vibrational-translational relaxation		
R166	$N_2(v) + N \leftrightarrow N_2(v' < v) + N$	$v = 1 \ldots 24$	33
R167	$N_2(v) + N_2 \leftrightarrow N_2(v-1) + N_2$	$v = 1 \ldots 24$	34
R168	$H_2(v) + H_2 \leftrightarrow H_2(v-1) + H_2$	$v = 1 \ldots 14$	11
R169	$H_2(v) + H \leftrightarrow H_2(v-1) + H$	$v = 1 \ldots 14$	18 [1]
R170	$H_2(v) + H \leftrightarrow H_2 + H$	$v = 1 \ldots 14$	18 [1]
R171	$N_2(v) + H_2 \leftrightarrow N_2(v-1) + H_2$	$v = 1 \ldots 24$	18
R172	$N_2(v) + H \leftrightarrow N_2(v-1) + H$	$v = 1 \ldots 24$	18 [1]
R173	$N_2(v) + H \leftrightarrow N_2 + H$	$v = 1 \ldots 24$	18 [1]
	Vibrational-vibrational relaxation		
R174	$N_2(v+1) + N_2(w) \leftrightarrow N_2(v) + N_2(w+1)$	$v = 1 \ldots 24, w < v$	34
R175	$H_2(v+1) + H_2(w) \leftrightarrow H_2(v) + H_2(w+1)$	$v = 1 \ldots 14, w < v$	11
R176	$H_2(v) + N_2(w-1) \leftrightarrow H_2(v-1) + N_2(w)$	$v = 1 \ldots 14, w = 1 \ldots 24$	18
R177	$N_2(v) + H_2(w-1) \leftrightarrow N_2(v-2) + H_2(w)$	$v = 2 \ldots 24, w = 1 \ldots 24$	18

[1] Only the single quantum processes are included separately (R156 and R159), the multi quantum processes are included by an effective sum (R157 and R160).

Table S6. Surface reactions included in the plasma kinetics model. The ground state, vibrational levels and electronically excited states are indicated with X, V and E, respectively. The sticking coefficients, γ, diffusion energy barrier, E_d, and the activation energy, E_a, are given. For the rate coefficient expressions we refer to [3].

#	Reaction				Ref.
	Wall relaxation				
R178	$N_2(A^3)$	→	N_2	$\gamma = 1 \times 10^{-3}$	18
R179	$N_2(A^1)$	→	$N_2(B^3)$	$\gamma = 1 \times 10^{-3}$	18
R180	$H_2(E)$	→	H_2	$\gamma = 1 \times 10^{-3}$	18
R181	$N_2(V)$	→	$N_2(V-1)$	$\gamma = 4.5 \times 10^{-4}$	18
R182	$H_2(V)$	→	$H_2(V-1)$	$\gamma = 1 \times 10^{-4}$	18
	Direct adsorption				
R183	$N(X,E) + \text{Surface}$	→	$N(s)$	$\gamma = 1$	10
R184	$H + \text{Surface}$	→	$H(s)$	$\gamma = 1$	10
R185	$NH + \text{Surface}$	→	$NH(s)$	$\gamma = 1$	10
R186	$NH_2 + \text{Surface}$	→	$NH_2(s)$	$\gamma = 1$	10
	Eley-Rideal				
R187	$N(X,E) + N(s)$	→	N_2	$\gamma = 6 \times 10^{-3}$	10
R188	$H + H(s)$	→	H_2	$\gamma = 1.5 \times 10^{-3}$	10
R189	$N(X,E) + H(s)$	→	$NH(s)$	$\gamma = 1 \times 10^{-2}$	10
R190	$NH + H(s)$	→	$NH_2(s)$	$\gamma = 1 \times 10^{-2}$	10
R191	$H + N(s)$	→	$NH(s)$	$\gamma = 8 \times 10^{-3}$	10
R192	$H + NH(s)$	→	$NH_2(s)$	$\gamma = 8 \times 10^{-3}$	10
	Eley-Rideal: NH_3 formation				
R193	$NH_2 + H(s)$	→	NH_3	$\gamma = 1 \times 10^{-2}$	10
R194	$H + NH_2(s)$	→	NH_3	$\gamma = 8 \times 10^{-3}$	10
R195	$H_2(X,V) + NH(s)$	→	NH_3	$\gamma = 8 \times 10^{-4}$	10
	Langmuir-Hinshelwood				
R196	$N(s) + H(s)$	→	$NH(s)$	$E_a = 1.099$ eV, $E_d = 0.2$ eV	28
R197	$NH(s) + H(s)$	→	$NH_2(s)$	$E_a = 0.3$ eV, $E_d = 0.2$ eV	10
R198	$NH_2(s) + H(s)$	→	NH_3	$E_a = 0.2$ eV, $E_d = 0.2$ eV	10
	Dissociative adsorption				
R199	$N_2(X,V) + \text{Surface}$	→	$N(s) + N(s)$	See references	35,36
R200	$N_2(E) + \text{Surface}$	→	$N(s) + N(s)$	$\gamma = 1 \times 10^{-1}$	28
R201	$H_2(X) + \text{Surface}$	→	$H(s) + H(s)$	$\gamma = 1 \times 10^{-3}$	28
R202	$H_2(v=1) + \text{Surface}$	→	$H(s) + H(s)$	$\gamma = 1 \times 10^{-2}$	28
R203	$H_2(v=2) + \text{Surface}$	→	$H(s) + H(s)$	$\gamma = 5 \times 10^{-2}$	28
R204	$H_2(v \geq 3) + \text{Surface}$	→	$H(s) + H(s)$	$\gamma = 1 \times 10^{-1}$	28
R205	$H_2(E) + \text{Surface}$	→	$H(s) + H(s)$	$\gamma = 1$	28

The sticking coefficients (γ) for the wall relaxation of the vibrationally excited molecules were adopted from Gordiets et al.[18] The authors assumed $\gamma = 4.5 \times 10^{-4}$ for N_2(V) (Reaction R181) based on Black et al., who performed a detailed study on the deactivation coefficient of N_2(V=1) upon collisions with various surfaces, including stainless steel.[37] The value of $\gamma = 1 \times 10^{-4}$ for H_2(V) (R182) is based on Heidner et al., who considered multiple de-excitation channels in flow tube experiments.[38] The relaxation of N_2(E) (specifically metastable N_2, R178 and R179) was estimated by Gordiets et al. upon comparison between their predictions and experiments.[18] Relaxation of H_2(E) (R180) is assumed equal, after Hong et al.[28]

Direct adsorption sticking coefficients (R183-R186) are adopted from Carrasco et al. who selected $\gamma = 1$ as a generally high value representing transition metals [10].

The Eley-Rideal (ER) sticking probability of $\gamma = 1.5 \times 10^{-3}$ between H and H(s) (R188) was adopted from Carrasco et al. who used the value yielding best agreement in their earlier experimental study, in which the apparatus had stainless steel walls.[10,39] The value of $\gamma = 6 \times 10^{-3}$ for N_2 (R187) was estimated by Carrasco et al.[10] The remaining sticking probabilities of ER type reactions (R189-R195) were adopted from the same study, where the values were chosen based on agreement with experimental data, due to a lack of reported values. Specifically, the ER reaction with H_2 as the gas phase reactant (R195) was chosen as significantly lower (order of magnitude 10^{-4} compared to $10^{-2} \dots 10^{-3}$). Note that Hong et al. report three unique sets of sticking probabilities for three types of surfaces (aluminium oxide, nanodiamond coated alumina and metal).[28]

The diffusion energy barrier of 0.2 eV for Langmuir-Hinshelwood (LH) type reactions (R196-R198) is adopted from Carrasco et al. who assumed this value based on the typical characteristics of chemisorbed H atoms on Fe.[10,28,40] The activation barrier for NH_2(s) formation (R197) was taken as 0.3 eV based on detailed surface kinetics studies,[41,42] while for the production of NH_3, a barrier of 0.2 eV was adopted.[10] For the elementary LH step between N(s) and H(s) (R196), an activation energy of 1.099 eV is used, after Hong et al.[28,41] They used the H atom diffusion barrier because the N atom diffusion barrier was reported as significantly higher (0.9 eV compared to 0.2 eV).[28]

The sticking coefficients for N_2 dissociative adsorption (R199) are resolved for the vibrational levels based on the studies by Hansen et al. Their calculations generally represent metallic surfaces.[35,36] The sticking probabilities of the dissociative adsorption of electronically excited N_2 and all H_2 molecules (R200-R205) were adopted from Hong et al., following their assumptions.[28] We assumed their H_2(v = 3) sticking probability also for any higher level (R204).

From the above, it is clear that the surface kinetics are subject to many assumptions and thus also to uncertainties. That includes the exact surface described. We summarize the above as a metal surface, most representative of iron, merely for reference and context. Indeed the exact surface characteristics, such as step or surface sites, are not captured. This would require a more detailed model, such as micro-kinetics models.[43–45] This type of model uses surface reaction rates derived from density functional theory calculations and generally solves those reaction rates in steady state conditions and does not include a full gas phase chemistry. To our knowledge, such micro-kinetics models have not yet been combined with a full time dependent plasma kinetics model. The present study, albeit with a less accurate surface description, focusses mainly on giving novel insight in the temporal discharge behaviour (i.e. the role of the micro-discharges and their afterglows). This study thus allows to better demarcate future studies, considering the increased number of degrees of freedom in a combined model (i.e. surface kinetics + plasma kinetics, introducing the exact surface, described by the surface binding energy).[43]

Nevertheless, the surface kinetics without radical-surface interactions (i.e. without radical adsorption and ER reactions) in our model provided similar NH_3 turnover frequencies as Mehta et al.[44] Indeed, our steady state NH_3 turnover frequencies are calculated to be 1.39×10^{-8} s^{-1} and 1.44×10^{-8} s^{-1} when vibrational dissociative adsorption is neglected and included, respectively. Considering that our surface kinetics are an approximation, we believe that this turnover frequency of 10^{-8} s^{-1} is in good agreement with the left side of the volcano plots by Mehta et al. (see figure S1: our results are indicated with a red dot).

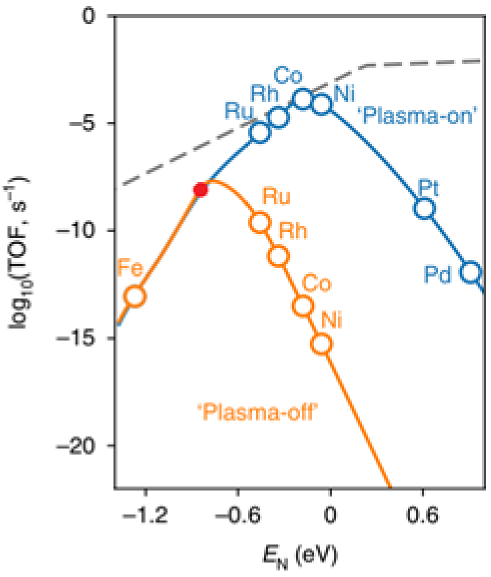

Figure S1. Comparison of our calculated turnover frequency (red dot) against the volcano curves of Mehta et al. Adapted by permission from Springer Nature: Nature Catalysis, Overcoming ammonia synthesis scaling relations with plasma-enabled catalysis, Mehta et al, 2018.

S.1.2. Translation of Experimentally Measured Current and Voltage Characteristics to the Model Conditions

We measured the charge-voltage characteristics, i.e. Lissajous figures, to (1) calculate the actual plasma current and gas voltage from the measured current and applied voltage, and (2) determine the partial discharging [46]. The Lissajous figures of the N_2/H_2 plasma are given in figure S2(a). In addition, in figure S2(b), the Lissajous figure for a measurement in pure argon is plotted, for which it is assumed that the plasma reactor is fully discharging [47]. With those figures, we can determine the dissipated plasma power, P_{diss}, and the partial discharging factor, β, using the following equations [46].

$$P_{diss} = W f_D \tag{S1}$$

$$W = 2U_b \Delta Q_D \tag{S2}$$

$$\Delta Q_D = \frac{Q_0}{1 - C_{cell}/C_{diel}} \tag{S3}$$

$$U_b = \left(1 + \frac{\alpha}{\beta}\frac{C_{cell}}{C_{diel}}\right)\Delta U \tag{S4}$$

$$\alpha + \beta = 1 \tag{S5}$$

$$\alpha = \frac{C_{diel} - \zeta_{diel}}{C_{diel} - C_{cell}} \tag{S6}$$

where W is the work done by the plasma, f_D is the discharge frequency, U_b is the burning voltage, ΔQ_D is the charge transferred by the discharge, Q_0 is the measured charge transferred, ΔU is the measured burning voltage, C_{diel} is the capacitance of the dielectric, C_{cell} is the capacitance of the reactor and ζ_{diel} is the effective dielectric capacitance.

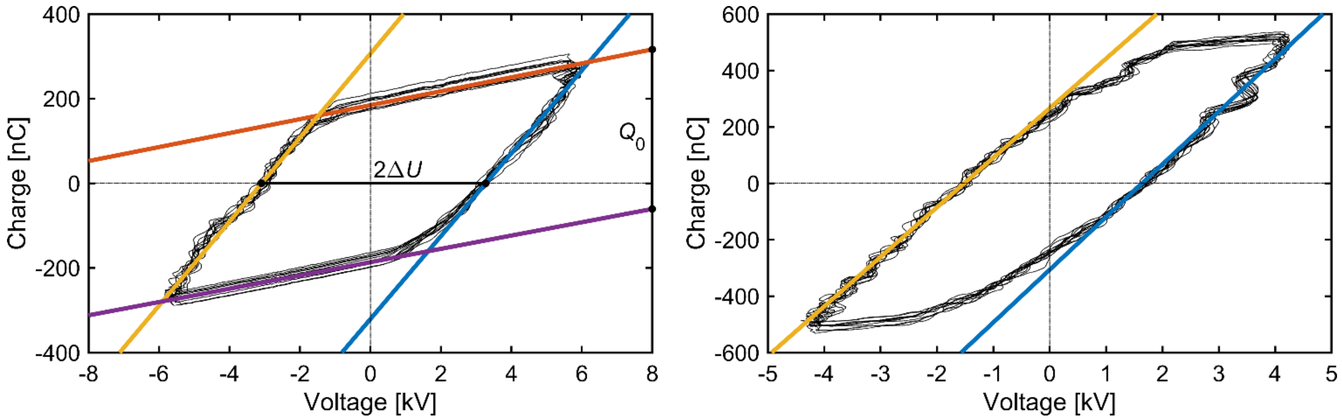

(a) (b)

Figure S2. Lissajous figure measured in our PB DBD and a 1:3 N_2:H_2 gas mixture (a) and operated with argon only (b). From those measurements, $\Delta U = 3066.7$ V and $Q_0 = 385.72$ nC are determined (a). The capacitances $\zeta_{diel} = 88.87$ pF and $C_{cell} = 16.468$ pF are determined from the two steepest and the two slighter slopes in (a), respectively. In addition $C_{diel} = 181.28$ pF is determined according to the plotted slopes in (b).

The plasma current i_{plasma} and gas voltage U_{gas} are given in figure S3, calculated with [46]

$$i_{plasma}(t) = \frac{1}{1 - C_{cell}/C_{diel}}\left[\frac{dQ(t)}{dt} - C_{cell}\frac{dV(t)}{dt}\right] \tag{S7}$$

$$U_{gas}(t) = \left(1 + \frac{\alpha}{\beta}\frac{C_{cell}}{C_{diel}}\right)V(t) - \frac{1}{\beta C_{diel}}Q(t) \tag{S8}$$

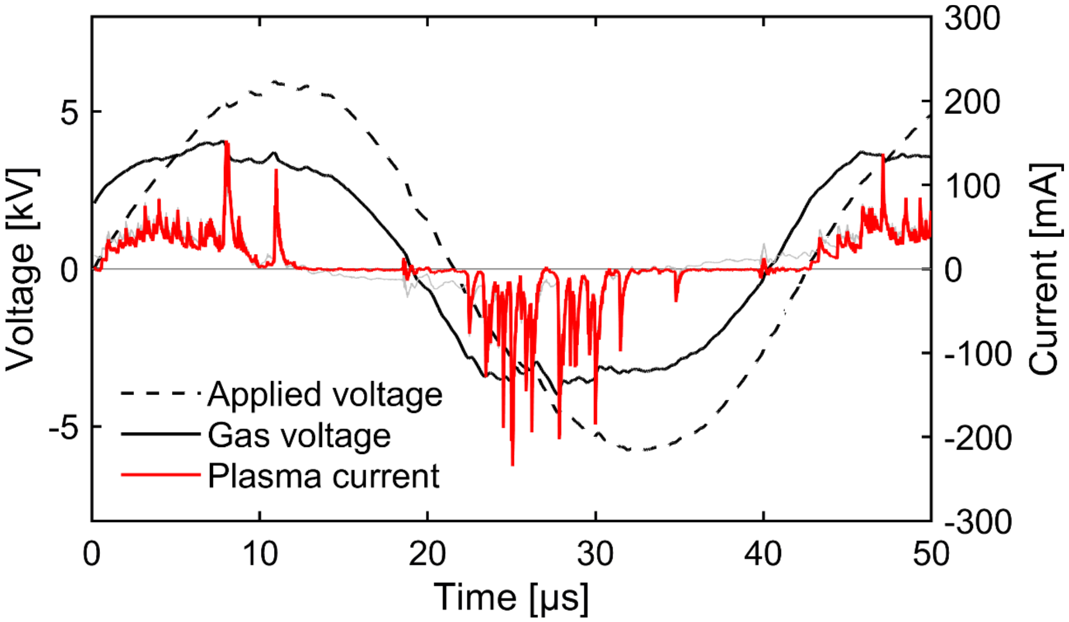

Figure S3. Plasma current and gas voltage, as well as the actual applied voltage, in our PB DBD and a 1:3 N_2:H_2 gas mixture.

The plasma current and gas voltage are used to calculate the instantaneous plasma power, which is shown in figure S4. Based on this figure (black line), we defined the average life-time of the micro-discharges as 200 ns (100 ns at FWHM), and we assume 25 micro-discharge per discharge half cycle.

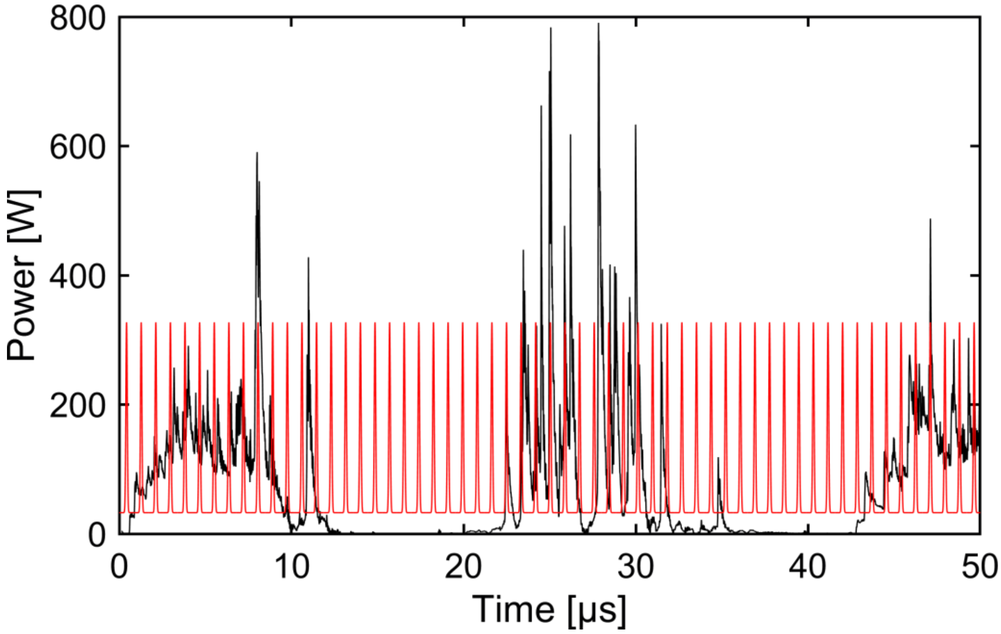

Figure S4. Instantaneous plasma power measured in our PB DBD and a 1:3 N_2:H_2 gas mixture, as well as the model representation of the instantaneous plasma power (red line).

The average instantaneous maximum power, i.e., if all micro-discharge peaks would be of the same height, is given by [3]

$$P_{max} = \frac{P_{diss}}{(1-\gamma)N_{MD}f_D\tau_{MD} + \gamma} \tag{S9}$$

$$P_{min} = \gamma P_{max}, \qquad \gamma \in [0,1] \tag{S10}$$

Where N_{MD} is the number of micro-discharges per discharge half cycle, f_D is the discharge frequency, τ_{MD} is the micro-discharge life-time, P_{max} and P_{min} are the average instantaneous maximum and minimum power, respectively, and γ is a distribution factor which defines the eventual minimum and maximum instantaneous power and power density (see section S.1.3 below). Table S7 summarizes all parameters introduced in section S.1.2, together with the values assumed in our model of the most relevant parameters.

Table S7. Summary of the parameters explained in section S.1.2.

Symbol	Description	Determination	Value	Units
P_{diss}	Average dissipated plasma power	Eq. S1	68	W
W	Work done by the plasma	Eq. S2		
f_D	Discharge frequency	Experiments	23.5	kHz
U_b	Burning voltage	Eq. S4		
ΔQ_D	Charge transferred by the discharge	Eq. S3		
Q_0	ΔQ_D, as measured	Figure S2(a)		
C_{cell}	Capacitance of the reactor	Figure S2(a)		
C_{diel}	Capacitance of the dielectric	Figure S2(b)		
α	Non-discharging fraction	Eq. S6		
β	Partial discharging fraction	Eq. S5	0.44	
ΔU	U_b, as measured	Figure S2(a)		
ζ_{diel}	Effective dielectric capacitance	Figure S2(a)		
N_{MD}	Number of micro-discharges per discharge half cycle	Figure S4	25	
τ_{MD}	Micro-discharge life time	Figure S4	200	ns
γ	Power distribution factor	Chosen	0.1	
P_{max}	Average maximum instantaneous power	Eq. S9	332	W
P_{min}	Average minimum instantaneous power	Eq. S10	33	W

It should be noted that the distribution factor, γ, is different from the definition in our previous work, in which we did not consider the experimentally measured instantaneous plasma power. With the more direct translation of the experimental current and voltage characteristics, we found that the relevant order of magnitude of the distribution factor is now in the range between 0.1 and 1, instead of between 10^{-6} and 1 as in our previous work [3]. We chose $\gamma = 0.1$, such that P_{max} is in reasonable agreement with the experimental measurement (cf. the red curve in figure S4). Lower γ values would result in very high P_{max}, i.e. 540 W for $\gamma = 0.01$.

Figure S4 represents all the micro-discharges (red line) over a time of 50 μs. In our model we consider an interpulse time of 76.8 ms, because the gas molecules do not feel all the micro-discharges when they travel through the reactor, i.e. we consider the number of micro-discharges of a single discharge period, but distributed over the longer gas residence time.

S.1.3. Relationship Between Instantaneous Power and Power Density: Choice of Discharge Volumes

The model description of the instantaneous power (cf. the red line in figure S4) consists of micro-discharge pulses and a constant, minimum, power value. We assign the latter to a uniform plasma component that is also present in between the micro-discharges. We thus need to define a discharge volume for both the micro-discharges and the uniform plasma. We assign the following volume to the uniform plasma:

$$V_U = \beta(1 - \alpha_{packing})V_R \tag{S11}$$

i.e., the uniform discharge volume, V_U, is the reactor volume, V_R, corrected for packing with the packing factor, $\alpha_{packing}$, as well as corrected for partial discharging of the plasma reactor, β. We chose $\alpha_{packing} = 0.68$, i.e. corresponding to a body-centred cubic structure, which is not the most optimal packing, but more likely to occur in practice. Indeed, the hexagonal close-packed structure, with $\alpha_{packing} = 0.74$, i.e. most optimal packing, is assumed to be unlikely. This was based on counting the number of beads in our reactor after the standard preparation procedure (e.g. including a vibrating step to ensure a dense packing). Equation S11 yields a uniform plasma discharge volume of 2.8 cm^3.

Furthermore, we attributed the size of typical voids in the assumed packed bed structure to the discharge volume of individual micro-discharges, such that the micro-discharge volume, V_{MD}, depends on the packing bead radius, r_{bead}

$$V_{MD} = \frac{4}{3}\pi(0.29r_{bead})^3 \tag{S12}$$

For a packing bead radius of 0.95 mm, Equation S12 yields a micro-discharge volume of 8.8×10^{-5} cm^3.

Using the above discharge volumes for the micro-discharges and the uniform plasma, we calculate the maximum and minimum power density in the model as 3.4×10^6 and 11.8 W/cm^3, respectively.

S.2. Surface Coverages and Gas Phase Concentrations in the Micro-Discharge

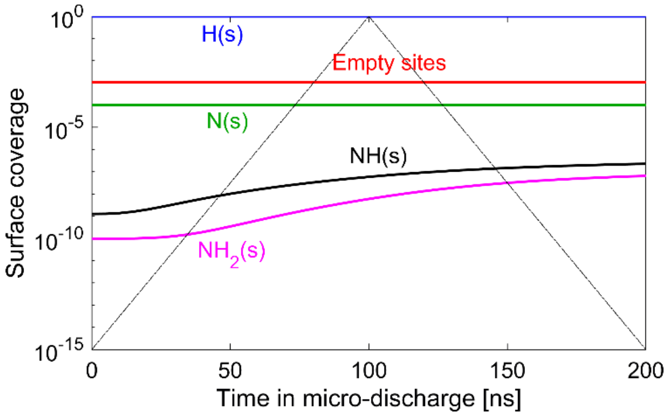

(a)

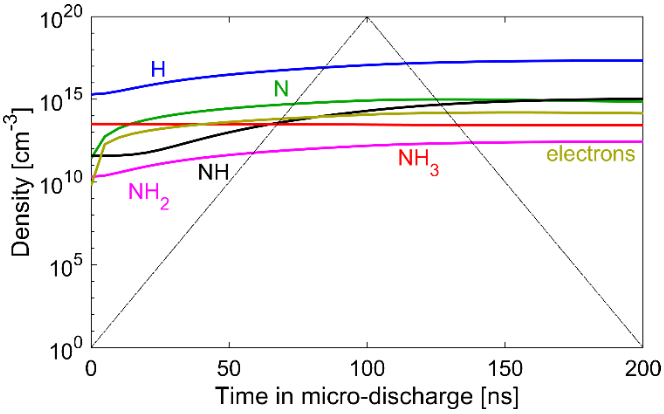

(b)

Figure S5. Surface coverages and fraction of empty surface sites (a), and concentrations of the neutral gas phase species and electrons (b), as a function of time in the first micro-discharge. This figure corresponds to figure 1 in the main paper.

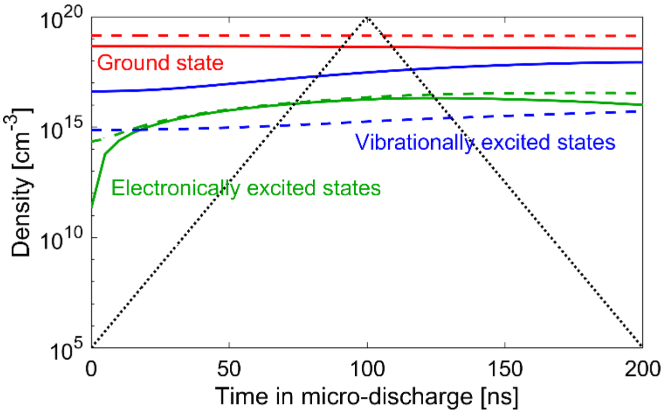

Figure S6. Number densities of the N_2 (solid lines) and H_2 (dashed lines) molecules in the ground state and the sum of the electronically and vibrationally excited states, as a function of time in the first micro-discharge. This figure corresponds to figure 2 in the main paper.

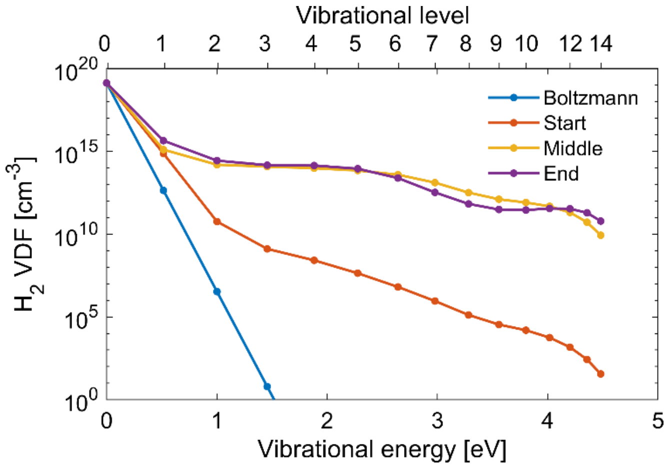

Figure S7. H_2 vibrational distribution function (VDF) at various moments in the micro-discharge, as well as the Boltzmann distribution at the gas temperature (400 K).

Table S8. Typical species densities in cm^{-3} of the various surface adsorbed species and plasma radicals in both the micro-discharge and afterglow. The equivalent coverages are given between brackets.

Species	**Micro-discharge (at maximum power density)**	**Afterglow (end)**
$NH_2(s)$	8.6×10^{8} (6.0×10^{-9})	6.1×10^{6} (4.3×10^{-11})
$NH(s)$	8.5×10^{9} (5.9×10^{-8})	3.0×10^{7} (2.1×10^{-10})
$H(s)$	1.4×10^{17} (1.0)	1.4×10^{17} (1.0)
$N(s)$	1.5×10^{13} (1.0×10^{-4})	2.4×10^{13} (1.7×10^{-4})
Surface	1.5×10^{14} (1.1×10^{-3})	1.4×10^{14} (9.9×10^{-4})
NH_3	2.9×10^{13}	6.9×10^{14}
NH_2	1.6×10^{12}	1.9×10^{12}
NH	2.0×10^{14}	1.5×10^{11}
H	1.2×10^{17}	1.0×10^{14}
N	8.4×10^{14}	8.1×10^{10}
H_2	1.4×10^{19}	1.4×10^{19}
N_2	4.3×10^{18}	4.6×10^{18}
e^-	1.2×10^{14}	1.2×10^{10}

S.3. Calculated Plasma Parameters

The N_2 vibrational temperature (figure S8(a)) is calculated to be slightly above 2100 K during the micro-discharges, and it relaxes back to above the gas temperature (700 K compared to 400 K) over approximately 1 ms. The H_2 vibrational temperature behaves similarly but reaches lower values, i.e. 600 K and 1100 K in the afterglow and micro-discharge, respectively. Figure S8(b) illustrates the calculated reduced electric field (E/N) and electron temperature (T_e), as a function of time. The maximum E/N was calculated to be 105 Td in each micro-discharge (and the maximum electron temperature was 5.9 eV. After the micro-discharges, both values significantly drop to virtually zero, but then rise again, and reach constant values in the entire afterglows, around E/N = 6 Td and T_e = 0.7 eV.

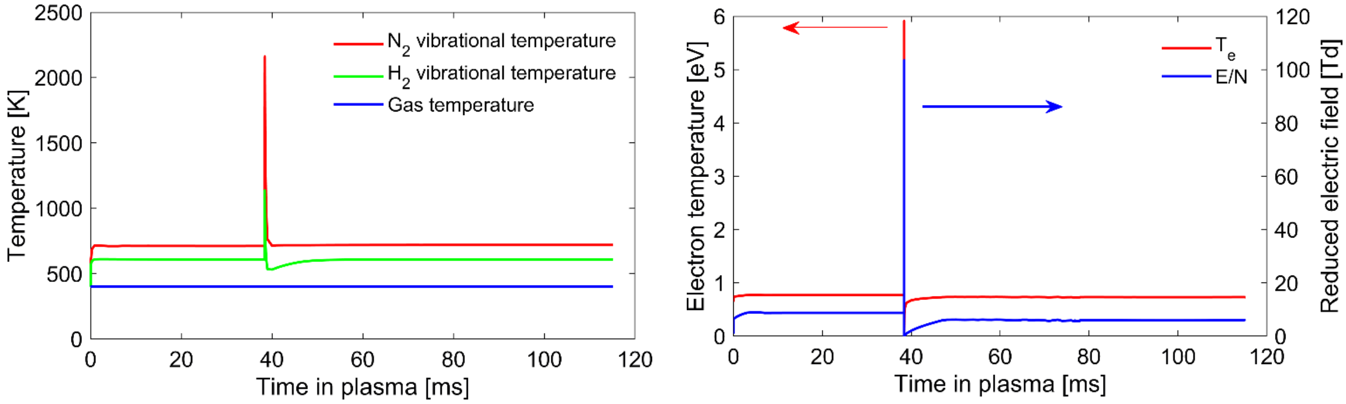

(a) (b)

Figure S8. N_2 and H_2 vibrational temperature (a) and reduced electric field and electron temperature (b) as a function of time in the plasma, from the start of the plasma to the end of the first micro-discharge and afterglow pair. The maximum values of the reduced electric field and electron temperature are 105 Td and 5.9 eV, respectively. The micro-discharge with a 200 ns duration takes place at 38.4 ms.

S.4. NH_3 Formation: Detailed Analysis of the Reaction Rates and Determination of the Rate-Limiting Step

Figure S9(a) depicts the actual reaction rates of the main NH_3 (and precursor) formation reactions as a function of time from the start of the plasma until the end of the first afterglow. The main NH_3 formation reaction is the elementary LH step of NH_2(s) with H(s); blue curve. Similarly, NH_2(s) is mainly formed from the LH reaction of NH(s) with H(s); red curve. NH(s), however, is formed from elementary ER steps, either by gas phase N with H(s), or by gas phase H with N(s); black curve in figure S9(a). This process is predominant in the micro-discharges (cf. figure S9(b)). In addition, we also plot the formation rate of NH_2(s) from gas phase NH and H(s) (ER mechanism; green curve), as it is also important in the micro-discharges (cf. figure S9(b)). Similarly, the ER formation of NH_3 by NH_2 and H(s) is also plotted (dark yellow curve), becoming important in the late afterglow.

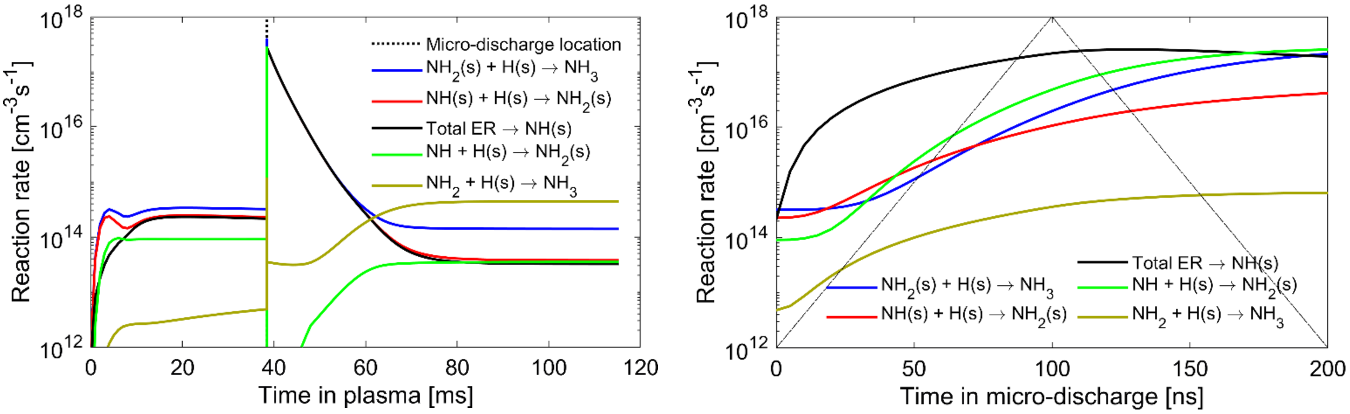

(a) (b)

Figure S9. Main reaction rates for the formation of NH_3, $NH_2(s)$ and NH(s) as a function of time in the plasma, from the start of the plasma to the end of the first micro-discharge and afterglow pair (a), and as a function of time in the first micro-discharge (b). “Total ER → NH(s)” stands for the sum of both reactions N + H(s) and H + N(s) reactions. In (a) the blue, red and black curve mostly overlap with each other. In (a), the micro-discharge with a 200 ns duration takes place at 38.4 ms.

Directly after the micro-discharge, we see in figure S9(a) a complete overlap between the reactions forming NH_3, $NH_2(s)$ and NH(s) (blue, red and black curves). This means that the intermediate products, NH(s) and $NH_2(s)$, are immediately converted towards NH_3. During the micro-discharges, there is no overlap between the various reaction rates, and the earlier products are generally formed at a higher rate (black and green curves are higher than blue curve). Note that in addition to the reactions in figure S9(b), NH_3 is net destroyed during the micro-discharges due to electron impact dissociation (cf. figure 2 in the main paper). Towards the end of the afterglow, the NH_3 formation is faster than the $NH_2(s)$ formation, and the latter is slightly faster than NH(s) formation, meaning that both $NH_2(s)$ and NH(s) are slightly being depleted in the afterglow, as discussed in section 3.2 in the main paper.

To find the rate-limiting step, we further investigate the formation of NH(s) in figure S10, where we plot the rates of the individual ER reaction steps as a function of time, again from the start of the plasma until the end of the first afterglow (figure S10(a)) and in the micro-discharge (figure S10(b)). The ER reaction of N with H(s) is generally faster, especially in the micro-discharges, and generally determines the total NH(s) formation, except before the first micro-discharge, where the ER reaction of H with N(s) seems more important. This is attributed to the relatively high dissociation of H_2 at the very beginning (see figure S13 below).

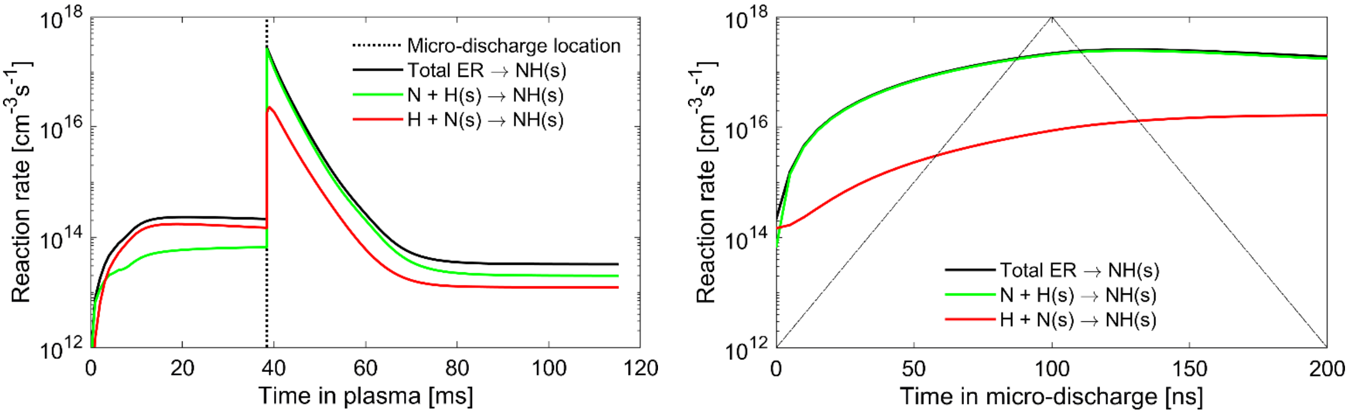

(a) (b)

Figure S10. Reaction rates for the formation of NH(s) as a function of time in the plasma, from the start of the plasma to the end of the first micro-discharge and afterglow pair (a), and as a function of time in the first micro-discharge (b). In (a), the micro-discharge with a 200 ns duration takes place at 38.4 ms.

Based on figures S9 and S10, we can identify the elementary ER reaction step between N and H(s) as the limiting reaction in NH_3 formation, i.e. N_2 dissociation in the plasma and H_2 or H (dissociative) adsorption are required for this. Similarly, the alternative ER reaction requires N(s). In figure S11, we show that the rate of this reaction overlaps with the direct adsorption of N, shortly after the micro-discharge. Thus, N atoms are required in both NH(s) formation pathways.

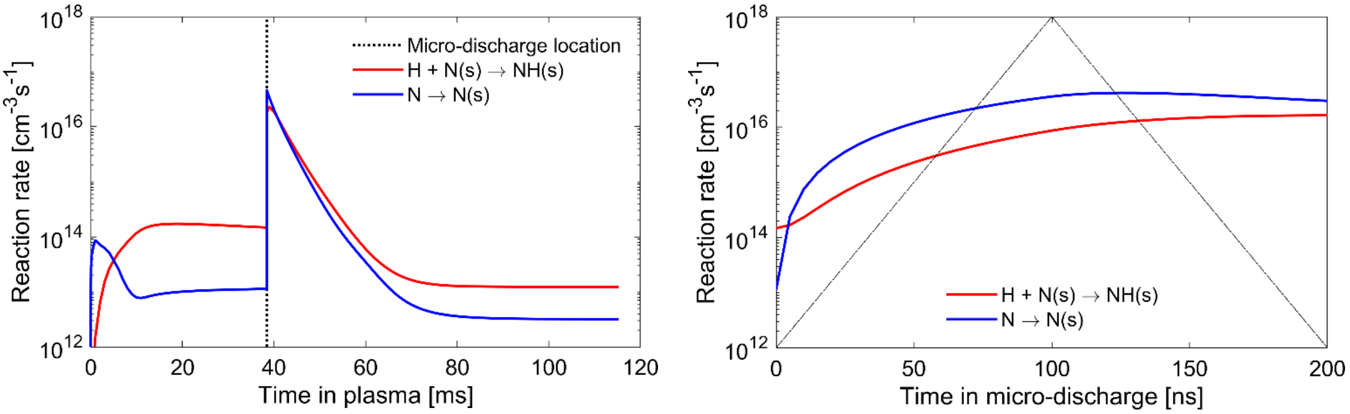

(a) (b)

Figure S11. Reaction rates for the formation and consumption of N(s) as a function of time in the plasma, from the start of the plasma to the end of the first micro-discharge and afterglow pair (a), and as a function of time in the first micro-discharge (b). In (a), the micro-discharge with a 200 ns duration takes place at 38.4 ms.

Unlike N(s), which is only significantly formed by direct adsorption and only reacts further to the desired products (NH(s)), the formation and consumption of H(s) is more complex. In the afterglow, we found that the net H(s) formation rate, attributed to direct adsorption (red curve in figure S12) overlaps in the afterglow with the total H(s) consumption rate to the desired products (blue curve). The contributions of individual processes to the net H(s) formation is given in figure S13.

During the micro-discharges (figure S12(b) and S13(b)), more H(s) is destroyed than formed. Indeed, this is due to the importance of H + H(s) → H_2. The dissociative adsorption (H_2 → 2 H(s)) has the lowest reaction rate once a micro-discharge occurred and the net formation of H_2 is then always higher, this means that the net H(s) formation is not determined by the dissociative adsorption anymore. However, the H(s) coverage is never significantly influenced after the initial coverage, due to the predominant dissociative adsorption before the first micro-discharge, and it is always nearly 1 (cf. figure 1(a) in the main paper and figure S5(a)).

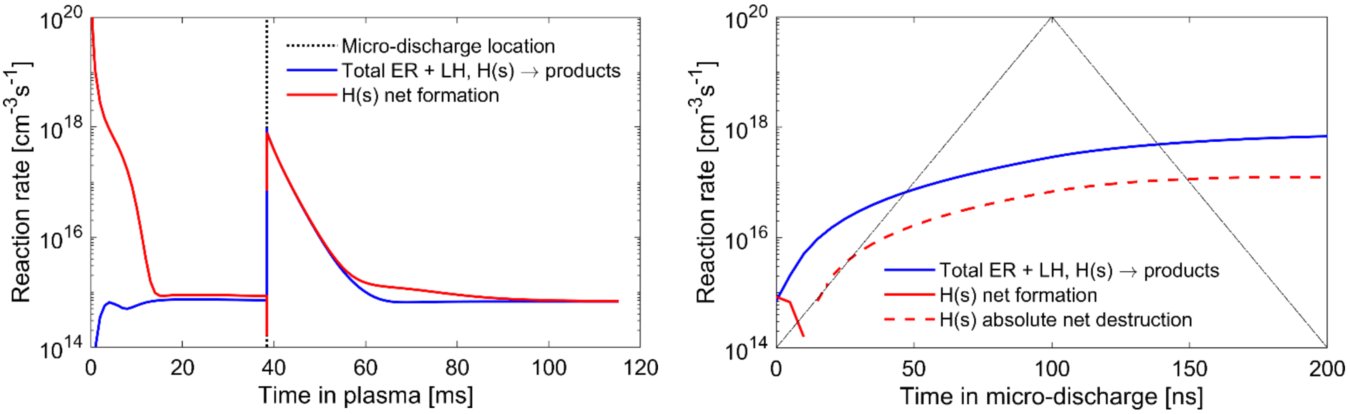

(a) (b)

Figure S12. Total and net reaction rates for the formation and consumption of H(s) as a function of time in the plasma, from the start of the plasma to the end of the first micro-discharge and afterglow pair (a), and as a function of time in the first micro-discharge (b). In (a), the micro-discharge with a 200 ns duration takes place at 38.4 ms.

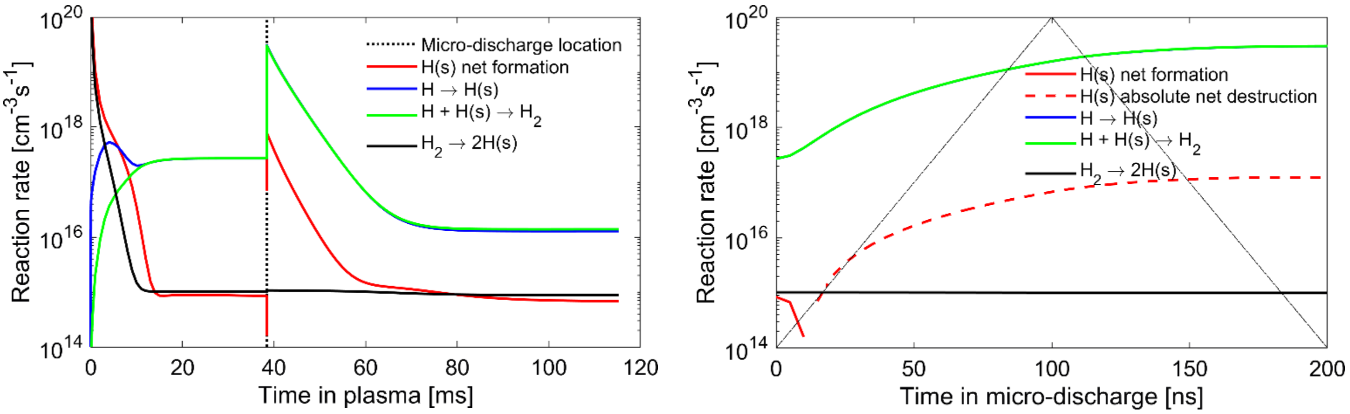

(a) (b)

Figure S13. Net formation of H(s) and the individual reactions that determine the net formation as a function of time in the plasma, from the start of the plasma to the end of the first micro-discharge and afterglow pair (a), and as a function of time in the first micro-discharge (b). The green and blue curves generally overlap (i.e., H → H(s) and H + H(s) → H_2). In (a), the micro-discharge with a 200 ns duration takes place at 38.4 ms.

We show in figure S14 the rates of direct adsorption of N and H atoms and compare it to the dissociation rates of N_2 and H_2. The dissociation rates of both N_2 and H_2 (i.e., upon electron impact) exhibit a sharp peak in the micro-discharge (red curves), followed by a pronounced drop, because the electric field reduces to near 0 directly after the micro-discharge (cf. section S.3 above). In the micro-discharges, the H_2 dissociation rate is 3 orders of magnitude higher, and consequently H adsorption is also 3 orders of magnitude faster than N adsorption. Directly after the micro-discharges, the ER reaction between H and N(s) (green dashed curve) clearly overlaps with direct adsorption of N (blue solid line). The dissociation of H_2 eventually overlaps with the direct adsorption of H in the afterglows (red and blue dashed lines), while the N_2 dissociation overlaps more with the ER reaction between N and H(s) (red and green solid lines). However, due to the quenching of H(s) back to H_2, we need to consider the net formation of H(s). This reaction rate is higher than for the ER reaction between N and H(s) (green curve). Instead, the net H(s) formation overlaps with the sum of all the ER and LH reactions that lead towards NH_3 and which require H(s) (cf. figure S12(a)).

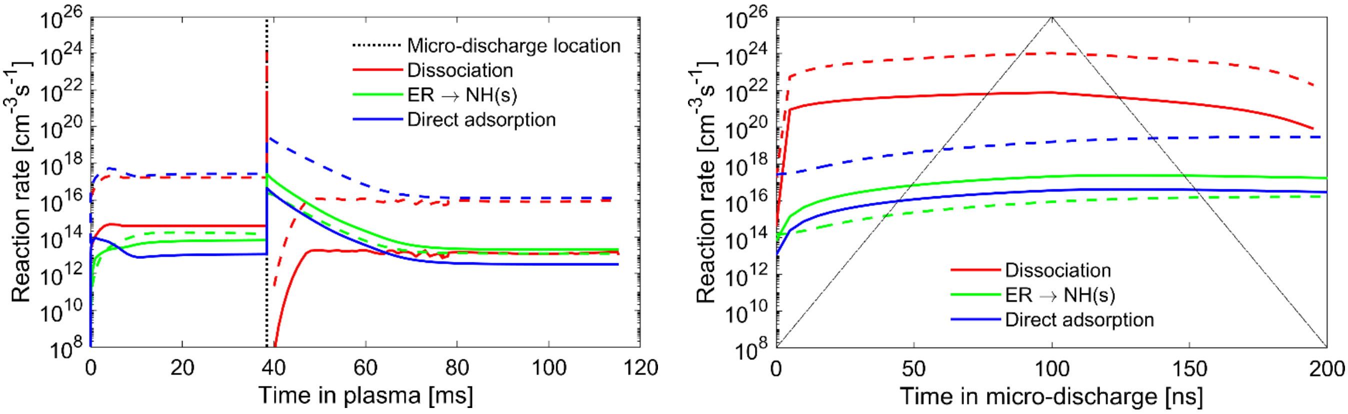

(a) (b)

Figure S14. Gas phase dissociation and atomic adsorption reaction rates for nitrogen (solid lines) and hydrogen (dashed lines) as a function of time in the plasma, from the start of the plasma to the end of the first micro-discharge and afterglow pair. The curves of "ER → NH(s)" are defined according the gas phase atom, i.e. N + H(s) is the solid curve and H + N(s) is the dashed curve. In (a), the micro-discharge with a 200 ns duration takes place at 38.4 ms.

Based on the above, we identify the adsorption of N and H atoms, both in ER reactions and direct adsorption, as rate-limiting. Consequently, electron impact dissociation of N_2 or H_2 in the plasma can be the overall rate-limiting step. In order to further specify the rate-limiting step, we performed calculations in which the rate coefficients for the atomic adsorption processes or for electron impact gas phase dissociation are multiplied by a factor 2. The adjusted reactions are listed in table S10 and the results are compared in figure S15.

Table S9. The test cases to confirm the rate-limiting reaction step. In each case the rate coefficient of the listed reactions was multiplied by a factor two.

Case	**Modified reactions**
Reference	None
Increased H_2 dissociation	$e^- + H_2(X,V) \rightarrow e^- + H + H$
Increased H atom adsorption	$H + Surface \rightarrow H(s)$ $H + H(s) \rightarrow H_2$ $H + N(s) \rightarrow NH(s)$ $H + NH(s) \rightarrow NH_2(s)$ $H + NH_2(s) \rightarrow NH_3$
Increased N_2 dissociation	$e^- + N_2(X,E,V) \rightarrow e^- + N + N$
Increased N atom adsorption	$N + Surface \rightarrow N(s)$ $N + H(s) \rightarrow NH(s)$ $N + N(s) \rightarrow N_2$

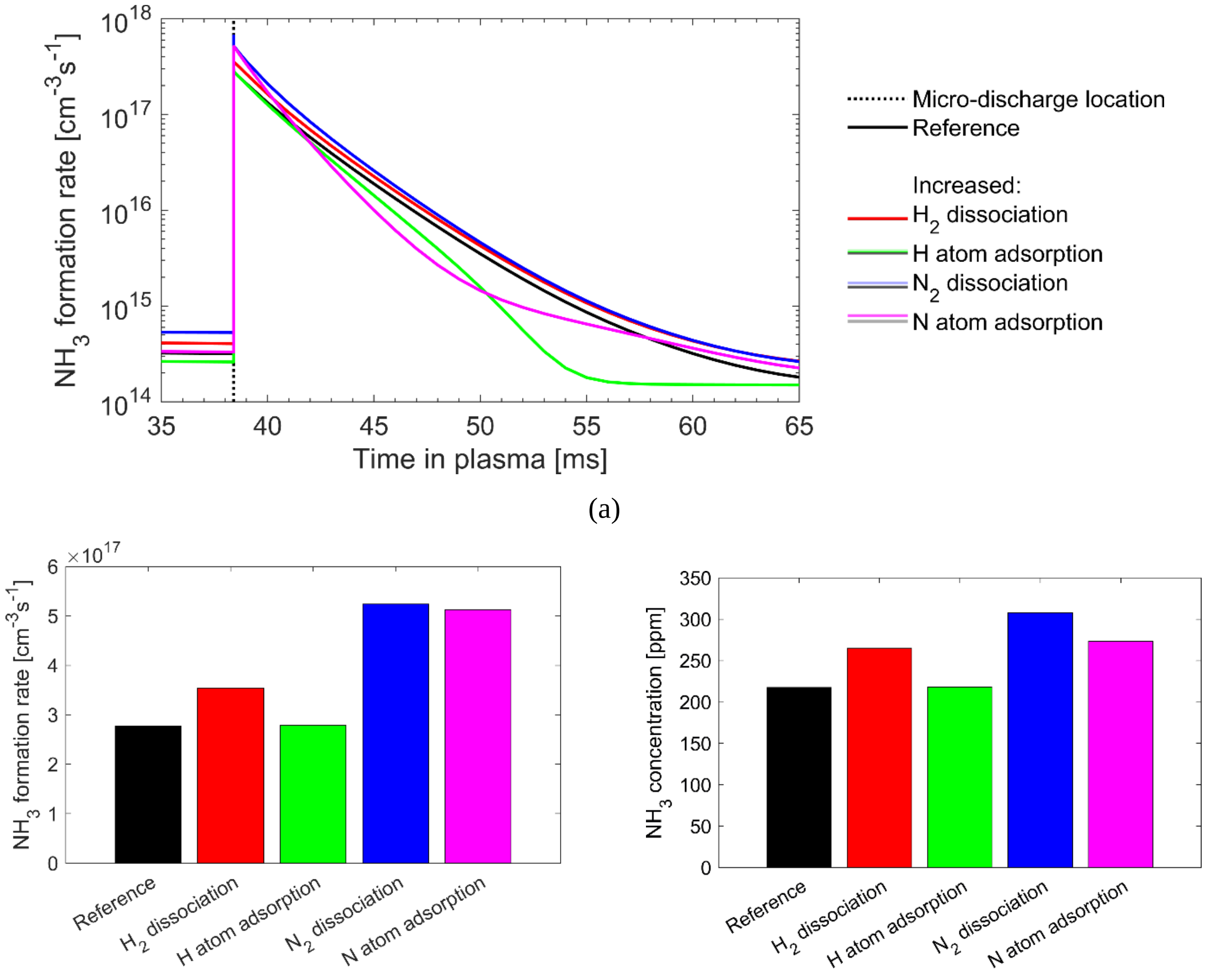

(a)

(b)

(c)

Figure S15. Comparisons of the various test cases presented in table S8 in which we increase the rate coefficients of specific reactions by a factor 2 (cf. table S8), showing the effect on the NH_3 formation rate, i.e. the reaction rate of $NH_2(s) + H(s) \rightarrow NH_3$, as a function of time (a), and 15 μs after the micro-discharge (b), and the eventual NH_3 concentration (c). In (a), the micro-discharge with a 200 ns duration takes place at 38.4 ms.

It is clear from figure S15(a) that the increased rate coefficient of the feed gas dissociation and of the atomic adsorption influences the final NH_3 synthesis reaction step ($NH_2(s) + H(s) \rightarrow NH_3$). Most notably, the slope of the increased N adsorption is steeper, due to faster depletion of gas phase N atoms. Only an increased H atom adsorption does not increase the NH_3 formation rate throughout the afterglow, which is attributed to the faster H atom recombination rate by $H + H(s) \rightarrow H_2$.

In figure S15(b) the NH_3 formation rates are compared shortly after the micro-discharge. Clearly both an increase in N_2 dissociation and N atom adsorption by a factor 2 effectively enhance the NH_3 formation rate by the same factor 2, directly after the micro-discharge. However, as noted before, the NH_3 formation rate with increased N atom adsorption rates will fall below the reference, due to the faster depletion of N atoms in the gas. An increase in the H_2 dissociation by a factor 2 also enhances the NH_3 formation rate, but only by a factor

1.3, due to a slight increase in H(s), and thus all further hydrogenation processes on the surface (N + H(s) → NH(s), NH(s) + H(s) → NH_2(s) and NH_2(s) → NH_3). The increase by a factor 1.3, instead of 2, approximately follows by considering all these three hydrogenation processes (i.e., $\sqrt[3]{2} = 1.26$).

In figure S15(c) the eventual NH_3 concentration is shown. Here the factor 2 increase is not directly reflected, due to how steady state is reached, i.e. because the overall system is non-linear in time. An increased gas phase H_2 dissociation enhances the NH_3 concentration by a factor 1.22. N atom adsorption increases the NH_3 concentration slightly more (factor 1.27), mainly due to an increase in N + H(s) → NH(s). H atom adsorption does not increase the NH_3 formation rate and the eventual NH_3 concentration is equal. The largest benefit is seen from an increased electron impact N_2 dissociation in the gas phase, enhancing the NH_3 concentration by a factor 1.41.

Based on the above analysis, electron impact N_2 dissociation in the plasma, followed by N atom adsorption at the surface, is identified as the rate-limiting step determining the NH_3 yield. H_2 dissociation in the plasma can also increase the formed NH_3, but to a lesser extent, as the H(s) precursor is required in multiple reaction steps. In addition, the surface is always generally covered with H(s) (see figure 1(a) in the main paper) and H_2 is easier to dissociate than N_2 (i.e. a dissociation threshold of 4.5 eV and 9.8 eV, respectively), thus the rate-limiting behaviour of the NH_3 synthesis in a DBD is attributed to nitrogen.

S.5. N_2 Dissociative Adsorption Compared Against N Atom Direct Adsorption

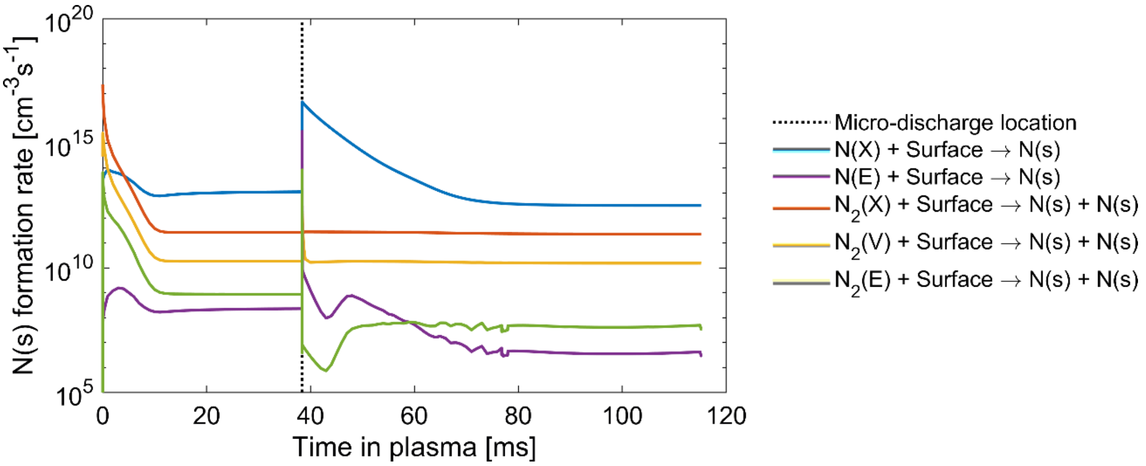

Figure S16. Comparison of N(s) formation rates from the various atomic adsorption and dissociative adsorption processes, resolved for the ground state species (X), electronically excited states (E) and vibrational levels (V), as a function of time in the plasma, from the start of the plasma to the end of the first micro-discharge and afterglow pair. The micro-discharge with a 200 ns duration takes place at 38.4 ms.

S.6. Data Used in the Assessment of the Reaction Mechanisms

We present the data based on which we assessed the reaction mechanisms presented in the main paper. We based ourself on the N_xH_y gas phase species (i.e. N, H, NH, NH_2 and NH_3), the surface adsorbed and related species (i.e. Surface (free sites), N(s), H(s) NH(s) and NH_2(s)) and the electrons and feed gas (i.e. e^- and H_2 and N_2, respectively). In addition, any other relevant species that is dictated by the significant reactions are also presented (i.e. electronically excited molecules: H_2(E) and N_2(E) and ions: N_2^+, H_2^+, N_2H^+ and H_3^+). We first considered separately whether or not the species is produced or destroyed during the micro-discharge and during the afterglow (cf. also figure 4 in the main paper). The reaction rates, source terms and the reactions themselves were carefully inspected to determine whether or not the single reaction could be considered, and if indeed only the production or destruction had to be considered during a single phase of the discharge (i.e. the micro-discharges and their afterglows).

The above analysis was based on the relative information instead of the absolute rates, i.e. the production-to-destruction ratio and the contribution of a reaction to either the production or destruction of a specific species. This is because the total source terms, and thus the typical reaction rates, can differ by orders of magnitude between the various species (cf. figure 4 and 5 in the main paper). In table S10 and S11 we present the reactions and their contribution to either the production or destruction of a species during the micro-discharge and the afterglow, respectively. In addition we note how we considered the species, based on the production-to-destruction ratio. The (individual) vibrational levels of both the N_2 and H_2 molecules, as well as the N_2 electronic states, N_2(E), are not resolved in table S9 of the micro-discharges, as those species typically show fast excitation and de-excitation processes between the various levels or states. Similarly, in addition in the afterglow (table S10), the H_2(X) and N_2(X) ground states are populated (and depopulated) by the various vibrational interactions and (de-)excitation processes and H_2(E) is mainly quenched back to the feed gas. Those interactions were not considered in detail, however typical vibrational distribution functions were shown in figure 3 and S6 for N_2 and H_2, respectively.

For context, we provide the reaction rates of the listed reactions in table S12, time averaged over the first micro-discharge and over the afterglow. Some reactions were not explicitly mentioned in the main paper (numbered in the tables with n.a.), those reactions typically quench any desired product back to the feed gas or indicate the population of electronically excited states or vibrational levels, which lead to the subsequent interactions between those states or levels.

Table S10. The various species considered in the assessment of the reaction mechanisms and the most significant reactions and their contribution to the production $(+)$ and/or destruction $(-)$ of this species in the micro-discharges. Either the production, destruction or both are given, depending on the specific consideration made, which is based on the production-to-destruction ratio (P/D).

Species	Consideration	(# main paper) Reaction	Contribution
$NH_2(s)$	Most significantly produced (P/D = 1.8)	$(13)\ NH + H(s) \rightarrow NH_2(s)$ $(19)\ NH(s) + H(s) \rightarrow NH_2(s)$	$0.86\ (+)$ $0.14\ (+)$
$NH(s)$	Most significantly produced (P/D = 12)	$(16)\ N + H(s) \rightarrow NH(s)$	$0.84\ (+)$
$H(s)$	Produced and destroyed (P/D = 0.98)	$(14)\ H + \mathrm{Surface} \rightarrow H(s)$ $(15)\ H + H(s) \rightarrow H_2$	$1.00\ (+)$ $0.98\ (-)$
$N(s)$	Most significantly produced (P/D = 3.2)	$(17)\ N + \mathrm{Surface} \rightarrow N(s)$	$0.96\ (+)$
Surface	Produced and destroyed (P/D = 1.01)	$(15)\ H + H(s) \rightarrow H_2 + \mathrm{Surface}$ $(14)\ H + \mathrm{Surface} \rightarrow H(s)$	$0.99\ (+)$ $1.00\ (-)$
NH_3	Most significantly destroyed (P/D = 0.08)	$(21)\ e^- + NH_3 \rightarrow e^- + NH_2 + H$ $(22)\ e^- + NH_3 \rightarrow e^- + NH + H_2$	$0.56\ (-)$ $0.32\ (-)$
NH_2	Produced and destroyed (P/D = 18)	$(21)\ e^- + NH_3 \rightarrow e^- + NH_2 + H$	$0.92\ (+)$
NH	Most significantly produced (P/D = 3.1)	$(12)\ N + H_2(E) \rightarrow H + NH$	$0.99\ (+)$
H	Most significantly produced (P/D = 421)	$(6)\ e^- + H_2(X, V, E) \rightarrow e^- + H + H$ $(10)\ N_2(E) + H_2 \rightarrow N_2 + H + H$	$0.89\ (+)$ $0.10\ (+)$
N	Most significantly produced (P/D = 1.4)	$(5)\ e^- + N_2(X, V, E) \rightarrow e^- + N + N$	$0.78\ (+)$
$H_2(X)$	Most significantly destroyed (P/D = 0.03)	$(6)\ e^- + H_2(X) \rightarrow e^- + H + H$ $(11)\ e^- + H_2 \rightarrow e^- + H_2(E)$	$0.63\ (-)$ $0.27\ (-)$
$H_2(E)$	Most significantly produced (P/D = 6.0)	$(11)\ e^- + H_2 \rightarrow e^- + H_2(E)$	$1.00\ (+)$
$N_2(X)$	Most significantly destroyed (P/D = 0.13)	$(\mathrm{n.a.})\ e^- + N_2(X) \rightarrow e^- + N_2(V)$	$0.94\ (-)$
e^-	Most significantly produced (P/D = 3.1)	$(7)\ e^- + N_2 \rightarrow e^- + e^- + N_2^+$ $(8)\ e^- + H_2 \rightarrow e^- + e^- + H_2^+$	$0.65\ (+)$ $0.17\ (+)$
N_2^+	Produced and destroyed (P/D = 1.00)	$(7)\ e^- + N_2 \rightarrow e^- + e^- + N_2^+$ $(\mathrm{n.a.})\ e^- + N_2(E) \rightarrow e^- + e^- + N_2^+$ $(28)\ N_2^+ + H_2 \rightarrow N_2H^+ + H$	$0.52\ (+)$ $0.44\ (+)$ $0.98\ (-)$
H_2^+	Produced and destroyed (P/D = 1.00)	$(8)\ e^- + H_2 \rightarrow e^- + e^- + H_2^+$ $(27)\ H_2^+ + H_2 \rightarrow H_3^+ + H$ $(\mathrm{n.a.})\ H_2^+ + N_2 \rightarrow N_2H^+ + H$	$1.00\ (+)$ $0.76\ (-)$ $0.24\ (-)$
H_3^+	Most significantly produced (P/D = 5.8)	$(27)\ H_2^+ + H_2 \rightarrow H_3^+ + H$	$1.00\ (+)$
N_2H^+	Most significantly produced (P/D = 2.1)	$(28)\ N_2^+ + H_2 \rightarrow N_2H^+ + H$ $(\mathrm{n.a.})\ H_2^+ + N_2 \rightarrow N_2H^+ + H$	$0.67\ (+)$ $0.33\ (+)$

Table S11. The various species considered in the assessment of the reaction mechanisms and the most significant reactions and their contribution to the production $(+)$ and/or destruction $(-)$ of this species in the afterglows of the micro-discharges. Either the production, destruction or both are given, depending on the specific consideration made which is based on the production-to-destruction ratio (P/D).

Species	**Consideration**	**(# main paper) Reaction**	**Contribution**
$NH_2(s)$	Produced and destroyed (P/D = 1.00)	$(19)\ NH(s) + H(s) \rightarrow NH_2(s)$	$0.99\ (+)$
		$(20)\ NH_2(s) + H(s) \rightarrow NH_3$	$1.00\ (-)$
$NH(s)$	Produced and destroyed (P/D = 1.00)	$(16)\ N + H(s) \rightarrow NH(s)$	$0.86\ (+)$
		$(18)\ H + N(s) \rightarrow NH(s)$	$0.14\ (+)$
		$(19)\ NH(s) + H(s) \rightarrow NH_2(s)$	$1.00\ (-)$
$H(s)$	Produced and destroyed (P/D = 1.00)	$(14)\ H + \mathrm{Surface} \rightarrow H(s)$	$1.00\ (+)$
		$(15)\ H + H(s) \rightarrow H_2$	$0.98\ (-)$
$N(s)$	Produced and destroyed (P/D = 1.1)	$(17)\ N + \mathrm{Surface} \rightarrow N(s)$	$1.00\ (+)$
		$(18)\ H + N(s) \rightarrow NH(s)$	$1.00\ (-)$
Surface	Produced and destroyed (P/D = 1.00)	$(15)\ H + H(s) \rightarrow H_2 + \mathrm{Surface}$	$0.98\ (+)$
		$(14)\ H + \mathrm{Surface} \rightarrow H(s)$	$1.00\ (-)$
NH_3	Most significantly produced (P/D = 8.7)	$(20)\ NH_2(s) + H(s) \rightarrow NH_3$	$0.88\ (+)$
NH_2	Produced and destroyed (P/D = 1.00)	$(21)\ e^- + NH_3 \rightarrow e^- + NH_2 + H$	$0.29\ (+)$
		$(\mathrm{n.a.})\ N + H_2 + M \rightarrow NH_2 + M$	$0.66\ (+)$
		$(\mathrm{n.a.})\ H + NH_2 \rightarrow H_2 + NH$	$0.33\ (-)$
		$(\mathrm{n.a.})\ N + NH_2 \rightarrow N_2 + H_2$	$0.19\ (-)$
		$(\mathrm{n.a.})\ N + NH_2 \rightarrow N_2 + H + H$	$0.19\ (-)$
		$(23)\ NH_2 + H(s) \rightarrow NH_3$	$0.10\ (-)$
NH	Produced and destroyed (P/D = 0.97)	$(12)\ N + H_2(E) \rightarrow H + NH$	$0.99\ (+)$
		$(\mathrm{n.a.})\ H + NH \rightarrow N + H_2$	$0.98\ (-)$
H	Most significantly destroyed (P/D = 0.14)	$(14)\ H + \mathrm{Surface} \rightarrow H(s)$	$0.35\ (-)$
		$(15)\ H + H(s) \rightarrow H_2$	$0.35\ (-)$
		$(\mathrm{n.a.})\ H + H + H_2 \rightarrow H_2 + H_2$	$0.13\ (-)$
		$(\mathrm{n.a.})\ H + NH \rightarrow N + H_2$	$0.13\ (-)$
N	Produced and destroyed (P/D = 0.98)	$(\mathrm{n.a.})\ H + NH \rightarrow N + H_2$	$1.00\ (+)$
		$(12)\ N + H_2(E) \rightarrow H + NH$	$0.96\ (-)$
e^-	Most significantly destroyed (P/D = 0.008)	$(24)\ e^- + H_3^+ \rightarrow H_2 + H$	$0.30\ (-)$
		$(25)\ e^- + H_3^+ \rightarrow H + H + H$	$0.30\ (-)$
		$(26)\ e^- + N_2H^+ \rightarrow N_2 + H$	$0.37\ (-)$
N_2^+	Produced and destroyed (P/D = 0.98)	$(\mathrm{n.a.})\ N_2(E) + N_2(E) \rightarrow N_2^+ + N_2 + e^-$	$1.00\ (+)$
		$(28)\ N_2^+ + H_2 \rightarrow N_2H^+ + H$	$0.98\ (-)$
H_2^+	Most significantly destroyed (P/D = 0.008)	$(27)\ H_2^+ + H_2 \rightarrow H_3^+ + H$	$0.78\ (-)$
		$(\mathrm{n.a.})\ H_2^+ + N_2 \rightarrow N_2H^+ + H$	$0.21\ (-)$
H_3^+	Most significantly destroyed (P/D = 3×10^{-6})	$(24)\ e^- + H_3^+ \rightarrow H_2 + H$	$0.50\ (-)$
		$(25)\ e^- + H_3^+ \rightarrow H + H + H$	$0.50\ (-)$
N_2H^+	Most significantly destroyed (P/D = 0.0002)	$(26)\ e^- + N_2H^+ \rightarrow N_2 + H$	$1.00\ (-)$

Table S12. The time averaged reaction rates, of the reactions in table S10 and S11, during a micro-discharge and its afterglow.

	Reaction rate ($\mathrm{cm^{-3}s^{-1}}$), time averaged over the:	
(# main paper) Reaction	**Micro-discharge**	**Afterglow**
(4) $\mathrm{H_2 + Surface \rightarrow H(s) + H(s)}$	1.01×10^{15}	9.46×10^{14}
(5) $\mathrm{e^- + N_2(X, V, E) \rightarrow e^- + N + N}$	4.63×10^{21}	1.19×10^{13}
(6) $\mathrm{e^- + H_2(X, V, E) \rightarrow e^- + H + H}$	4.81×10^{23}	7.72×10^{15}
(7) $\mathrm{e^- + N_2 \rightarrow e^- + e^- + N_2^+}$	1.78×10^{20}	7.80×10^{6}
(8) $\mathrm{e^- + H_2 \rightarrow e^- + e^- + H_2^+}$	6.84×10^{20}	3.65×10^{7}
(9) $\mathrm{e^- + N_2 \rightarrow e^- + N_2(E)}$	2.45×10^{23}	6.41×10^{15}
(10) $\mathrm{N_2(E) + H_2 \rightarrow N_2 + H + H}$	5.59×10^{22}	1.64×10^{16}
(11) $\mathrm{e^- + H_2 \rightarrow e^- + H_2(E)}$	2.04×10^{23}	1.81×10^{15}
(12) $\mathrm{N + H_2(E) \rightarrow H + NH}$	7.81×10^{21}	4.17×10^{17}
(13) $\mathrm{NH + H(s) \rightarrow NH_2(s)}$	8.77×10^{16}	3.89×10^{13}
(14) $\mathrm{H + Surface \rightarrow H(s)}$	1.55×10^{19}	1.17×10^{18}
(15) $\mathrm{H + H(s) \rightarrow H_2}$	1.55×10^{19}	1.15×10^{18}
(16) $\mathrm{N + H(s) \rightarrow NH(s)}$	1.49×10^{17}	7.36×10^{15}
(17) $\mathrm{N + Surface \rightarrow N(s)}$	2.57×10^{16}	1.30×10^{15}
(18) $\mathrm{H + N(s) \rightarrow NH(s)}$	8.46×10^{15}	1.18×10^{15}
(19) $\mathrm{NH(s) + H(s) \rightarrow NH_2(s)}$	1.47×10^{16}	8.51×10^{15}
(20) $\mathrm{NH_2(s) + H(s) \rightarrow NH_3}$	5.57×10^{16}	8.60×10^{15}
(21) $\mathrm{e^- + NH_3 \rightarrow e^- + NH_2 + H}$	1.36×10^{19}	8.54×10^{14}
(22) $\mathrm{e^- + NH_3 \rightarrow e^- + NH + H_2}$	7.73×10^{18}	1.88×10^{14}
(23) $\mathrm{NH_2 + H(s) \rightarrow NH_3}$	3.40×10^{14}	3.09×10^{14}
(24) $\mathrm{e^- + H_3^+ \rightarrow H_2 + H}$	4.29×10^{19}	5.53×10^{14}
(25) $\mathrm{e^- + H_3^+ \rightarrow H + H + H}$	4.29×10^{19}	5.53×10^{14}
(26) $\mathrm{e^- + N_2H^+ \rightarrow N_2 + H}$	2.30×10^{20}	6.85×10^{14}
(27) $\mathrm{H_2^+ + H_2 \rightarrow H_3^+ + H}$	5.19×10^{20}	3.36×10^{9}
(28) $\mathrm{N_2^+ + H_2 \rightarrow N_2H^+ + H}$	3.38×10^{20}	1.38×10^{11}
(n.a.) $\mathrm{H + NH_2 \rightarrow H_2 + NH}$	1.63×10^{17}	9.67×10^{14}
(n.a.) $\mathrm{N + NH_2 \rightarrow N_2 + H_2}$	1.43×10^{17}	5.75×10^{14}
(n.a.) $\mathrm{N + NH_2 \rightarrow N_2 + H + H}$	1.43×10^{17}	5.75×10^{14}
(n.a.) $\mathrm{e^- + N_2(E) \rightarrow e^- + e^- + N_2^+}$	1.53×10^{20}	4.98×10^{8}
(n.a.) $\mathrm{H_2^+ + N_2 \rightarrow N_2H^+ + H}$	1.64×10^{20}	9.23×10^{8}
(n.a.) $\mathrm{N + H_2 + M \rightarrow NH_2 + M}$	1.06×10^{15}	1.94×10^{15}
(n.a.) $\mathrm{H + NH \rightarrow N + H_2}$	2.51×10^{21}	4.25×10^{17}
(n.a.) $\mathrm{H + H + H_2 \rightarrow H_2 + H_2}$	5.03×10^{18}	2.23×10^{17}

The data presented in table S10 and S11 also gives some insight in the sensitivity of the overall assessed reaction mechanisms to changes in the underlying rate coefficients of either the involved reactions themselves or of other reactions also present in the chemistry set (cf. table S1-S6). Indeed, reaction rate coefficients always have an uncertainty, typically in the order of 30%.[48,49] In general, if we concluded that there is only one significant reaction relevant to the production or destruction of one species, while the contribution of this reaction is just slightly above 0.5 (i.e. 50%), then it is clear that a slight change in this or other reactions could change the actual main reaction taking place. On the other hand, if we find a large contribution to the overall production or destruction (i.e. contributions of 0.8, or 80%, and up), then it is less likely that other reactions that were not part of our assessed reaction mechanisms (which thus have very low contributions) would become the most important, even when the uncertainties in the rate coefficients are considered. In table S10 and S11, the lowest considered contribution to the production or destruction of a species, for determining the reaction mechanisms, is 0.81, i.e. 81%, which is the sum of the four reactions (0.33 + 0.19 + 0.19 + 0.1) accounting for the destruction of NH_2 in the afterglow (cf. table S11).

S.7. Influence of Langmuir-Hinshelwood Reactions and Alternative Reaction Mechanisms

Because the adopted Langmuir-Hinshelwood activation energies are subject to uncertainties, we calculate several hypothetical cases in which we change the activation energy and thus the rate coefficients governing the reactions, as shown in table S13. The diffusion barrier is kept constant, as reported in table S6. We cover cases in which the reactions are slower and faster. Results are given in table S14.

Table S13. Summary of the calculations performed to investigate the influence of the LH reactions.

			Rate coefficient	
Case	**Reaction**	**Activation energy**	**cm^3s^{-1}**	**s^{-1}**
Adopted chemistry	$\mathrm{H(s)} + \mathrm{N(s)} \rightarrow \mathrm{NH(s)}$	$E_a = 1.099$ eV	7.5×10^{-22}	1.1×10^{-4}
	$\mathrm{H(s)} + \mathrm{NH(s)} \rightarrow \mathrm{NH_2(s)}$	$E_a = 0.3$ eV	8.8×10^{-12}	1.3×10^{6}
	$\mathrm{H(s)} + \mathrm{NH_2(s)} \rightarrow \mathrm{NH_3}$	$E_a = 0.2$ eV	1.6×10^{-10}	2.3×10^{7}
Equal barriers	$\mathrm{H(s)} + \mathrm{N(s)} \rightarrow \mathrm{NH(s)}$	$E_a = 1.0$ eV	1.3×10^{-20}	1.9×10^{-3}
	$\mathrm{H(s)} + \mathrm{NH(s)} \rightarrow \mathrm{NH_2(s)}$	$E_a = 1.0$ eV	1.3×10^{-20}	1.9×10^{-3}
	$\mathrm{H(s)} + \mathrm{NH_2(s)} \rightarrow \mathrm{NH_3}$	$E_a = 1.0$ eV	1.3×10^{-20}	1.9×10^{-3}
Increased barriers	$\mathrm{H(s)} + \mathrm{N(s)} \rightarrow \mathrm{NH(s)}$	$E_a = 2.0$ eV	3.3×10^{-33}	4.8×10^{-16}
	$\mathrm{H(s)} + \mathrm{NH(s)} \rightarrow \mathrm{NH_2(s)}$	$E_a = 2.0$ eV	3.3×10^{-33}	4.8×10^{-16}
	$\mathrm{H(s)} + \mathrm{NH_2(s)} \rightarrow \mathrm{NH_3}$	$E_a = 2.0$ eV	3.3×10^{-33}	4.8×10^{-16}
Barrierless	$\mathrm{H(s)} + \mathrm{N(s)} \rightarrow \mathrm{NH(s)}$	$E_a = 0.0$ eV	5.3×10^{-8}	7.6×10^{9}
	$\mathrm{H(s)} + \mathrm{NH(s)} \rightarrow \mathrm{NH_2(s)}$	$E_a = 0.0$ eV	5.3×10^{-8}	7.6×10^{9}
	$\mathrm{H(s)} + \mathrm{NH_2(s)} \rightarrow \mathrm{NH_3}$	$E_a = 0.0$ eV	5.3×10^{-8}	7.6×10^{9}

Table S14. Calculated steady state NH_3 concentration and NH_3 formation rate through the LH pathway ($\mathrm{H(s)} + \mathrm{NH_2(s)} \rightarrow \mathrm{NH_3}$) for the various test cases.

Case	**NH_3 concentration (ppm)**	**LH NH_3 formation rate ($cm^{-3}s^{-1}$) in the first afterglow**
Basic chemistry	223	$\underline{8.6 \times 10^{15}}$
Equal barriers	224	2.4×10^{10}
Increased barriers	224	6.0×10^{-3}
Barrierless	223	$\underline{8.7 \times 10^{15}}$

Table S14 lists the calculated steady-state NH_3 concentration for the basic model and the additional calculations. It can be seen that all additional calculations give the same concentration as the basic chemistry which was used to assess the reaction mechanisms in detail. In the basic chemistry model we found that the eventual formation of NH_3 is through the LH reaction: $\mathrm{H(s)} + \mathrm{NH_2}(s) \rightarrow \mathrm{NH_3}$. Table S14 also reports the corresponding reaction rate of this LH reaction. Despite the same NH_3 concentration, we do see different LH reaction rates when increasing the activation energy (i.e. for barriers of 1.0 eV and 2.0 eV in the case of equal barriers and increased barriers, respectively). This means that reactions other than this LH reaction should be responsible for the formation of NH_3. When the LH reactions were barrierless, the eventual rate is the same, despite a significantly higher rate coefficient (cf. table S13), thus indicating a preceding step as rate limiting, i.e. the formation of NH(s) by ER reactions. Indeed, also when the LH formation of NH(s) is increased, i.e. the barrierless case, the formation rate is still the same, indicating that the same ER NH(s) formation is still faster than the LH alternative.

In addition, when the LH reactions are slower (increased barriers), we don't see a change in the main formation of NH(s) by the ER reactions, but we do see other NH3 formation reactions taking place in the final step, with the same rate as when the formation was due to LH reactions, as shown in table S15.

Table S15. Comparison of the NH_3 formation rate by the most important reactions for the various test cases.

	NH_3 formation rate ($cm^{-3}s^{-1}$) in the first afterglow		
Case	$\mathbf{H(s) + NH_2(s) \rightarrow NH_3}$	$\mathbf{H_2 + NH(s) \rightarrow NH_3}$	$\mathbf{H + NH_2(s) \rightarrow NH_3}$
Basic chemistry	$\underline{8.6 \times 10^{15}}$	3.4×10^{13}	2.2×10^{11}
Equal barriers	2.4×10^{10}	$\underline{7.7 \times 10^{15}}$	7.6×10^{14}
Increased barriers	6.0×10^{-3}	$\underline{7.7 \times 10^{15}}$	7.6×10^{14}
Barrier-less	$\underline{8.7 \times 10^{15}}$	6.8×10^{8}	6.8×10^{8}

The reaction $\mathrm{H_2} + \mathrm{NH(s)} \rightarrow \mathrm{NH_3}$ is dominant when the LH reaction ($\mathrm{H(s)} + \mathrm{NH_2(s)} \rightarrow \mathrm{NH_3}$) is not fast enough, and is characterized by a nearly equal rate (underlined in table S15). We also list $\mathrm{H} + \mathrm{NH_2(s)} \rightarrow \mathrm{NH_3}$ which has the highest reaction rate after the LH reaction and the H_2 ER reaction in the basic chemistry case. Indeed, we also found that the stepwise ER hydrogenations with H are fast enough to account for the same NH_3 formation rates if the H_2 ER reaction is absent.

Based on the above we can present two alternative NH_3 formation paths as revealed by our model. After the ER formation of NH(s), a single reaction step might form NH_3:

$$\mathrm{H_2} + \mathrm{NH(s)} \rightarrow \mathrm{NH_3} \tag{S13}$$

Alternatively, stepwise ER hydrogenation reactions might form NH_3:

$$H + NH(s) \rightarrow NH_2(s) \tag{S14}$$

$$H + NH_2(s) \rightarrow NH_3 \tag{S15}$$

References

(1) Pancheshnyi, S.; Eismann, B.; Hagelaar, G. J. M.; Pitchford, L.C. Computer code ZDPlasKin, versions 2.0a; University of Toulouse: LAPLACE, CNRS-UPS-INP, Toulouse, France. http://www.zdplaskin.laplace.univ-tlse.fr (2008).

(2) Hagelaar, G. J. M.; Pitchford, L. C. Solving the Boltzmann Equation to Obtain Electron Transport Coefficients and Rate Coefficients for Fluid Models. *Plasma Sources Sci. Technol.* **2005**, *14*.

(3) van 't Veer, K.; Reniers, F.; Bogaerts, A. Zero-Dimensional Modelling of Unpacked and Packed Bed Dielectric Barrier Discharges: The Role of Vibrational Kinetics in Ammonia Synthesis. *Plasma Sources Sci. Technol.* **2020**, *29*, 045020.

(4) Kim, H.; Nanba, T. Atmospheric-Pressure Nonthermal Plasma Synthesis of Ammonia over Ruthenium Catalysts. *Plasma Process. Polym.* **2016**, 1–9.

(5) Alves, L. L. The IST-LISBON Database on LXCat. *J. Phys. Conf. Ser.* **2014**, *565*, 012007.

(6) Morgan database. https://nl.lxcat.net/ (accessed May, 2019).

(7) Tarnovsky, V.; Deutsch, H.; Becker, K. Cross-Sections for the Electron Impact Ionization of ND_x (x = 1−3). *Int. J. Mass Spectrom. Ion Process.* **1997**, *167–168*, 69–78.

(8) Itikawa, Y. Cross Sections for Electron Collisions with Nitrogen Molecules. *J. Phys. Chem. Ref. Data* **2005**, *35*, 31–53.

(9) Yoon, J.-S.; Song, M.-Y.; Han, J.-M.; Hwang, S. H.; Chang, W.-S.; Lee, B.; Itikawa, Y. Cross Sections for Electron Collisions with Hydrogen Molecules. *J. Phys. Chem. Ref. Data* **2008**, *37*, 913–931.

(10) Carrasco, E.; Jiménez-Redondo, M.; Tanarro, I.; Herrero, V. J. Neutral and Ion Chemistry in Low Pressure Dc Plasmas of H2/N2 Mixtures: Routes for the Efficient Production of NH_3 and NH_4^+. *Phys. Chem. Chem. Phys.* **2011**, *13*, 19561–19572.

(11) Capitelli, M.; Ferreira, C. M.; Gordiets, B. F.; Asipov, A. I. *Plasma Kinetic in Atmospheric Gases*; Springer-Verlag Berlin Heidelberg: Berlin, 2000.

(12) Nighan, W. L. Electron Energy Distributions and Collision Rates in Electrically Excited N_2, CO, and CO_2. *Phys. Rev. A* **1970**, *2*, 1989–2000.

(13) Kossyi, I. A.; Kostinsky, A. Y.; Matveyev, A. A.; Silakov, V. P. Kinetic Scheme of the Non-Equilibrium Discharge in Nitrogen-Oxygen Mixtures. *Plasma Sources Sci. Technol.* **1992**, *1*, 207–220.

(14) Celiberto, R.; Janev, R. K.; Wadehra, J. M.; Laricchiuta, A. Cross Sections for 14-eV e-H_2 Resonant Collisions: Dissociative Electron Attachment. *Phys. Rev. A* **2009**, *80*, 12712.

(15) Laporta, V.; Little, D. A.; Celiberto, R.; Tennyson, J. Electron-Impact Resonant Vibrational Excitation and Dissociation Processes Involving Vibrationally Excited N_2 Molecules. *Plasma Sources Sci. Technol.* **2014**, *23*, 065002.

(16) Kewley, D. J.; Hornung, H. G. Free-Piston Shock-Tube Study of Nitrogen Dissociation. *Chem. Phys. Lett.* **1974**, *25*, 531-536.

(17) Gaens, W. Van; Bogaerts, A. Kinetic Modelling for an Atmospheric Pressure Argon Plasma Jet in Humid Air. *J. Phys. D. Appl. Phys.* **2013**, *46*, 275201.

(18) Gordiets, B.; Ferreira, C. M.; Pinheiro, M. J.; Ricard, A. Self-Consistent Kinetic Model of Low-Pressure N_2–H_2 Flowing Discharges: I. Volume Processes. *Plasma Sources Sci. Technol.* **1998**, *7*, 363–378.

(19) Caridade, P. J. S. B.; Rodrigues, S. P. J.; Sousa, F.; Varandas, A. J. C. Unimolecular and Bimolecular Calculations for HN_2. *J. Phys. Chem. A* **2005**, *109*, 2356–2363.

(20) Fontijn, A.; Shamsuddin, S. M.; Crammond, D. Kinetics of the NH Reaction with H_2 and Reassessment of HNO Formation from NH + CO_2, H_2O. *Combust. Flame* **2006**, *145*, 543–551.

(21) Johnston, H. S. Computation of High-Temperature Rate Constants for Bimolecular Reactions of Combustion Products. *Symp. Combust.* **1967**, *11*, 837–844.

(22) Klippenstein, S. J.; Harding, L. B.; Ruscic, B.; Sivaramakrishnan, R.; Srinivasan, N. K.; Su, M.; Michael, J. V. Thermal Decomposition of NH_2OH and Subsequent Reactions: Ab Initio Transition State Theory and Reflected Shock Tube Experiments. *J. Phys. Chem. A* **2009**, *113*, 10241–10259.

(23) Sheets, D. Chemical Kinetic Data Sheets for High-Temperature Chemical Reactions. *J. Phys. Chem. Ref. Data* **1983**, *12*, 531.

(24) Deppe, J.; Friedrichs, G.; Ibrahim, A.; Romming, H.; Wagner, H. G. The Thermal Decomposition of NH_2 and NH Radicals. *Berichte der Bunsengesellschaft für Phys. Chemie* **1998**, *102*, 1474–1485.

(25) Hanson, R. K.; Salimian, S. Survey of Rate Constants in the N/H/O System. In *Combustion Chemistry*; Gardiner, W. C., Ed.; Springer New York: New York, 1984; pp 361–421.

(26) Clyne, M. A. A.; Stedman, D. H. Rate of Recombination of Nitrogen Atoms. *J. Phys. Chem.* **1967**, *71*, 3071–3073.

(27) Fridman, A. *Plasma Chemistry*; Cambridge University Press: Cambridge, U.K., 2008.

(28) Hong, J.; Pancheshnyi, S.; Tam, E.; Lowke, J. J.; Prawer, S.; Murphy, A. B. Kinetic Modelling of NH_3 Production in N_2–H_2 Non-Equilibrium Atmospheric-Pressure Plasma Catalysis. *J. Phys. D. Appl. Phys.* **2018**, *51*, 109501.

(29) Anicich, V. G. Evaluated Bimolecular Ion-Molecule Gas Phase Kinetics of Positive Ions for Use in Modeling Planetary Atmospheres, Cometary Comae, and Interstellar Clouds. *J. Phys. Chem. Ref. Data* **1993**, *22*, 1469–1569.

(30) Wang, W.; Snoeckx, R.; Zhang, X.; Cha, M. S.; Bogaerts, A. Modeling Plasma-Based CO_2 and CH_4 Conversion in Mixtures with N_2, O_2, and H_2O: The Bigger Plasma Chemistry Picture. *J. Phys. Chem. C* **2018**, *122*, 8704–8723.

(31) Celiberto, R.; Janev, R. K.; Wadehra, J. M.; Laricchiuta, A. Cross Sections for 11-14-eV e-H_2 Resonant Collisions: Vibrational Excitation. *Phys. Rev. A.* **2008**, *77*, 012714.

(32) Celiberto, R.; Janev, R. K.; Laporta, V.; Tennyson, J.; Wadehra, J. M. Electron-Impact Vibrational Excitation of Vibrationally Excited H_2 molecules Involving the Resonant ${}^2\Sigma_g^+$ Rydberg-Excited Electronic State. *Phys. Rev. A.* **2013**, *88*, 062701.

(33) Esposito, F. N–N_2 State to State Vibrational-Relaxation and Dissociation Rates Based on Quasiclassical Calculations. *Chem. Phys.* **2006**, *331*, 1–8.

(34) Adamovich, I. V; Rich, J. W.; Treanor, C. E. Vibrational Energy Transfer Rates Using a Forced Harmonic Oscillator Model. *J. Thermophys. Heat Transf.* **1998**, *12*, 57-65.

(35) Billing, D.; Guldberg, A.; He, N. E.; Hansen, F. Y. Dissociative Chemisorption of N_2 on Rhenium: Dynamics at Low Impact Energies. *Chem. Phys.* **1990**, *147*, 1–11.

(36) Hansen, F. Y.; Henriksen, N. E.; Billing, G. D.; Guldberg, A. Catalytic Synthesis of Ammonia Using Vibrationally Excited Nitrogen Molecules: Theoretical Calculation of Equilibrium and Rate Constants. *Surf. Sci.* **1992**, *264*, 225–234.

(37) Black, G.; Wise, H.; Schechter, S.; Sharpless, R. L.; Black, G.; Wise, H.; Schechter, S.; Sharpless, R. L. Measurements of Vibrationally Excited Molecules by Raman Scattering II. Surface Deactivation of Vibrationally Excited N_2. *J. Chem. Phys.* **1974**, *60*, 3526.

(38) Heidner, R. F.; Kasper, J. V. V. An Experimental Rate Constant for $H+H_2(v'' = 1) \rightarrow H+H_2\ (v'' = 0)$. *Chem. Phys. Lett.* **1972**, *15*, 179–184.

(39) Carrasco, E.; Herrero, V. J.; Tanarro, I. Isotopic Exchange Processes in Cold Plasmas of H_2/D_2 Mixtures. *Phys. Chem. Chem. Phys.* **2011**, *13*, 9655–9666.

(40) Barth, J. V. Transport of Adsorbates at Metal Surfaces: From Thermal Migration to Hot Precursors. *Surf. Sci. Rep.* **2000**, *40*, 75–149.

(41) Ertl, G. Surface Science and Catalysis- Studies on the Mechanism of Ammonia Synthesis: The P. H. Emmett Award Address. *Catal. Rev. Sci. Eng.* **1980**, *21*, 201–223.

(42) Dumesic, J. A.; Trevino, A. A. Kinetic Simulation of Ammonia Synthesis Catalysis. *J. Catal.* **1989**, *129*, 119–129.

(43) Engelmann, Y.; van ’t Veer, K.; Gorbanev, Y.; Neyts, E. C.; Schneider, W. F.; Bogaerts, A. Plasma Catalysis for Ammonia Synthesis: The Importance of Eley-Rideal Reactions. *Submitted.*

(44) Mehta, P.; Barboun, P.; Herrera, F. A.; Kim, J.; Rumbach, P.; Go, D. B.; Hicks, J. C.; Schneider, W. F. Overcoming Ammonia Synthesis Scaling Relations with Plasma-Enabled Catalysis. *Nat. Catal.* **2018**, *1*, 269–275.

(45) Engelmann, Y.; Mehta, P.; Neyts, E. C.; Schneider, W. F.; Bogaerts, A. Predicted Influence of Plasma Activation on Nonoxidative Coupling of Methane on Transition Metal Catalysts. *ACS Sustain. Chem. Eng.* **2020**, *8*, 6043–6054.

(46) Peeters, F. J. J.; Sanden, M. C. M. Van De. The Influence of Partial Surface Discharging on the Electrical Characterization of DBDs. *Plasma Sources Sci. Technol.* **2015**, *24*, 015016.

(47) Uytdenhouwen, Y.; Alphen, S. Van; Michielsen, I.; Meynen, V.; Cool, P.; Bogaerts, A. A Packed-Bed DBD Micro Plasma Reactor for CO_2 Dissociation: Does Size matter? *Chem. Eng. J.* **2018**, *348*, 557–568.

(48) Berthelot, A.; Bogaerts, A. Modeling of CO2 Plasma: Effect of Uncertainties in the Plasma Chemistry. *Plasma Sources Sci. Technol.* **2017**, *26*, 115002.

(49) Wang, W.; Berthelot, A.; Zhang, Q.; Bogaerts, A. Modelling of Plasma-Based Dry Reforming: How Do Uncertainties in the Input Data Affect the Calculation Results? *J. Phys. D. Appl. Phys.* **2018**, *51*, 204003.